Acquisition of auditory discrimination mediated by different processes through two distinct circuits linked to the lateral striatum

Susumu Setogawa[1,2,3,4,5,*], Takashi Okauchi[4], Di Hu[4], Yasuhiro Wada[6], Keigo Hikishima[7], Hirotaka Onoe[8], Kayo Nishizawa[3], Nobuyuki Sakayori[9], Hiroyuki Miyawaki[1,2], Takuma Kitanishi[2], Kenji Mizuseki[1,2], Yilong Cui[4], Kazuto Kobayashi[3*]

[1]Department of Physiology, Graduate School of Medicine, Osaka Metropolitan University, Osaka 545-8585, Japan

[2]Department of Physiology, Osaka City University Graduate School of Medicine, Osaka 545-8585, Japan

[3]Department of Molecular Genetics, Institute of Biomedical Sciences, Fukushima Medical University, Fukushima 960-1295, Japan

[4]Laboratory for Biofunction Dynamics Imaging, RIKEN Center for Biosystems Dynamics Research, Kobe 650-0047, Japan

[5]Japan Society for the Promotion of Science, Tokyo 102-0083, Japan

[6]Laboratory for Pathophysiological and Health Science, RIKEN Center for Biosystems Dynamics Research, Kobe 650-0047, Japan

[7]Medical Devices Research Group, Health and Medical Research Institute, National Institute of Advanced Industrial Science and Technology, Tsukuba 305-8564, Japan

[8]Human Brain Research Center, Kyoto University Graduate School of Medicine, Kyoto 606-8507, Japan

[9]Department of Physiology and Oral Physiology, Graduate School of Biomedical and Health Sciences, Hiroshima University, Hiroshima 734-8553, Japan

28 *Address for correspondence:

29 Kazuto Kobayashi, Ph.D.

30 E-mail: kazuto@fmu.ac.jp

31 Department of Molecular Genetics, Institute of Biomedical Sciences, Fukushima Medical

32 University, Fukushima 960-1295, Japan.

33 Tel. +81-24-547-1667

34

35 Susumu Setogawa, Ph.D.

36 E-mail: setogawa@omu.ac.jp

37 Department of Physiology, Graduate School of Medicine, Osaka Metropolitan University, Osaka

38 545-8585, Japan

39 Tel. +81-6-6645-3717

40

Abstract

The striatum, the central hub of cortico-basal ganglia loops, contains functionally heterogeneous subregions distinguished by the topographic patterns of structural connectivity. These subregions mediate various processes of procedural learning. However, it remains unclear when and how striatal subregions engage in the acquisition of sensory stimulus-based decision-making. A neuroimaging of regional brain activity shows that the anterior dorsolateral striatum (aDLS) and posterior ventrolateral striatum (pVLS) in rats are activated in a different temporal pattern during the acquisition phase of auditory discrimination. Chronic and transient pharmacologic manipulations show that the aDLS promotes the behavioral strategy driven by the stimulus-response association while suppressing that by the response-outcome association, and that the pVLS contributes to forming and maintaining the stimulus-response strategy. Electrophysiological recording indicates that subpopulations of aDLS neurons predominantly represent the outcome of specific behaviors at the initial period of discrimination learning, and that pVLS subpopulations encode the beginning and ending of each behavior according to the progress of learning. In addition, other subpopulations of striatal neurons indicate sustained activation after obtaining reward with distinct patterns reflecting the stimulus-response associations. Our findings demonstrate that aDLS and pVLS neurons integrate the new learning of auditory discrimination in spatiotemporally and functionally different manners.

Introduction

The neural network connecting the cerebral cortex, basal ganglia, and thalamus forms functionally heterogeneous loops distinguished by the topographic patterns of connectivity (***Alexander and Crutcher, 1990; Foster et al., 2021***), and is implicated in various learning processes by the integration of cognitive, sensorimotor, and reward information (***Kim and Hikosaka, 2015; Yin and Knowlton, 2006***). The striatum is a key node in the cortico-basal ganglia loops, and its segregated subregions are considered to mediate procedural learning, such as motor skills and instrumental behavior, through parallel processing via different loops (***Kupferschmidt et al., 2017; Thorn et al., 2010; Yin et al., 2009***). Previous studies in humans and non-human primates have reported that the neural activity within the striatum shifts from the associative subregions (caudate and anterior putamen) to the sensorimotor subregions (posterior putamen) as motor learning progresses (***Doyon et al., 2009; Lehéricy et al., 2005; Miyachi et al., 2002; Miyachi et al., 1997***). In rodents, an instrumental behavior initiates as goal-directed actions and then transits to stimulus-response habits (***Dickinson, 1995; O'Hare et al., 2016***), requiring the dorsomedial striatum (DMS; a homologue to the caudate in primates) and the dorsolateral striatum (DLS; a homologue to the putamen in primates), respectively (***Yin et al., 2004; Yin et al., 2005***). Based on these results, a model of procedural learning has been proposed, in which the functional dominance changes from the associative to sensorimotor subregions in the striatum during the learning phases (***Redgrave et al., 2010***).

In contrast, deviations from the prior model are evident in other behavioral tasks on decision-making based on external sensory cues. For example, the neural activity in the caudate in humans is associated with learning of a visuomotor association task and the execution of learned behavior (***Seger and Cincotta, 2005; Toni and Passingham, 1999***). The tail of the caudate in non-human primates contributes to the automatic, habitual behavior in decision-making task using complex visual stimuli (***Kim and Hikosaka, 2013***). In rodents, the DLS is involved in the acquisiton and execution of the discrimination task with visual and auditory cues, wheras the DMS

85 madiates the performance of learned behavior (***Featherstone and McDonald, 2004; Featherstone***
86 ***and McDonald, 2005***). Moreover, other striatal subregions, such as the posterior striatum and
87 ventrolateral striatum in rodents are also engaged in the auditory discrimination (***Guo et al., 2019;***
88 ***Lee et al., 2020; Xiong et al., 2015***). Based on these results, a hypothesis has arisen that the
89 acquisition of sensory cue-based decision-making requires wide-range spatiotemporal processing
90 within the striatum. However, the neural mechanism by which the functional circuits linked to
91 striatal subregions change throughout learning processes is not yet fully understood.
92 To investigate a large-scale striatal reorganization in accordance with the acquisition of
93 external cue-dependent decisions, we conducted a two-alternative auditory discrimination task with
94 rats (***Nishizawa et al., 2012***). Using a small-animal neuroimaging technique, we found that the
95 anterior dorsolateral striatum (aDLS) and posterior ventrolateral striatum (pVLS) are activated to
96 the highest level at the middle and late stages during the acquisition phase of auditory
97 discrimination, respectively. Then, chronic pharmacologic manipulations confirmed that the aDLS
98 and pVLS are necessary for discrimination learning, and the transient manipulations also indicated
99 the function of these subregions in the learning at the corresponding stages. The resultant effects of
100 the manipulations on the behavioral strategy showed that the aDLS promotes the strategy based on
101 the stimulus-response association, while suppressing that based on response-outcome associations.
102 Additionally, the pVLS engages in the formation and maintenance of the stimulus-response
103 association strategy. Electrophysiological data of striatal neurons indicated the presence of aDLS
104 subpopulations, mainly representing the outcome of specific behaviors at the initial period of
105 auditory discrimination and pVLS subpopulations encoding the beginning and ending of behavior
106 in association with the development of the discrimination. There were other subpopulations in the
107 aDLS and pVLS showing long-term increased activity following reward with different patterns of
108 the combination between the stimulus and response. These findings revealed that the two striatal
109 subregions are involved in the acquisition of auditory discrimination through distinct spatiotemporal
110 and functional fashions, challenging the prior model which proposed a transition from the

associative to sensorimotor striatal subregions during learning.

Results

Leaning processes of auditory discrimination

We employed a two-alternative auditory discrimination task, in which rats are required to make new associations between a tone instruction cue (high frequency tone of 10 kHz or low frequency tone of 2 kHz) and a response (pressing the right or left lever) (***Nishizawa et al., 2012***), setting the interval between the stimulus presentation and lever insertion to 3 s (***Figure 1A***). The success rate gradually increased, reaching a plateau around Day 13, which persisted through Day 24 (***Figure 1B***). Based on changes observed in the success rate, we categorized the learning processes into two phases: the acquisition phase, which lasted until Day 13; and the learned phase, which began after Day 13 and then continued at least until Day 24. In addition, we divided the acquisition phase into three stages depending on the success rate that included the early (< 60%), middle (60–80%), and late (80–100%) stages. We chose Days 2, 6, and 10 at the early, middle, and late stages in the acquisition phase, respectively, as well as Days 13 and 24 in the learned phase for statistical comparison of the success rate. There were significant differences between Days 2 and 6, Days 6 and 10, as well as Days 10 and 13, showing no significant difference between Days 13 and 24 (***Figure 1C***). In contrast, the response time and omission rate did not vary among the training days (***Figure 1D and E***), and the variation of response bias decreased along with the progress of auditory discrimination (***Figure 1F***).

Distinct brain activity patterns in striatal subregions during learning processes

To investigate dynamic changes in regional brain activity in the entire striatum during auditory discrimination in the same animals, we conducted the positron emission tomography (PET) for small animals with 2-deoxy-2-[^{18}F]fluoro-D-glucose (^{18}F-FDG), which measures cerebral glucose metabolism correlated to brain activity (***Cui et al., 2015; Kornblum et al., 2000; Zimmer et al.,***

137 ***2017***) (***Figure 2A***). Before the auditory discrimination task, we performed the single lever press
138 task, in which a lever pseudorandomly presented on either the left or right side, and the rats learned
139 to press a lever associated with receiving a reward. This task was used as a control that does not
140 require the decision process based on the auditory stimulus. ^{18}F-FDG-PET scanning was carried out
141 on Day 4 of the single lever press task, and then during a series of training sessions including the
142 acquisition (Days 2, 6, and 10) and learned (Day 24) phases (***Figure 2B***). The average number of
143 lever presses in the single lever press task exceeded 80 times (81.6 ± 1.3, mean ± s.e.m.) on Day 2
144 and maintained that level until Day 4 (***Figure 2C***). In the following auditory discrimination task, the
145 success rate gradually increased along with the training days (***Figure 2D***), showing a significant
146 difference among sessions in which we performed the ^{18}F-FDG-PET scanning (***Figure 2E***). The
147 response time and omission rate were consistent among the days, and the variation of response bias
148 became smaller as the task progresses (***Figure 2E***). These performances were similar to those in the
149 intact rats (compared to ***Figure 1C–F***), suggesting that the procedure for ^{18}F-FDG-PET scans does
150 not affect the acquisition of discrimination.

151 We investigated the brain regions, in which ^{18}F-FDG uptake significantly increased or
152 decreased during the learning processes, applying a statistical significance threshold ($p < 0.001$,
153 uncorrected) and an extent threshold, by using a voxel-based statistical parametric analysis (***Cui et***
154 ***al., 2015***). We first analyzed task-related brain activity by comparing ^{18}F-FDG uptake on either day
155 of the discrimination task with that on Day 4 of the single lever press task (summarized in ***Figure***
156 ***2–table supplement 1***). In the striatal subregions, there were significant increases of the activity in
157 the unilateral aDLS and the bilateral pVLS on Days 6 and 10, respectively (***Figure 2F and G***).
158 However, no significant change was observed in the DMS during the acquisition phase except a
159 unilateral decrease on Day 24 (***Figure 2F***). Next, to evaluate the activity related to the progress of
160 learning, ^{18}F-FDG uptake on Days 6, 10, and 24 was compared with that on Day 2. The learning-
161 dependent brain activity was significantly increased in the bilateral aDLS and the unilateral pVLS
162 on Days 6 and 10, respectively (***Figure 2H***), whereas the activity decreased in the bilateral DMS on

163 Day 24 (***Figure 2H***). This decrease was also detected when ^{18}F-FDG uptakes were compared
164 between Days 10 and 24 (***Figure 2H***), suggesting the down-regulation of the DMS activity in the
165 learned phase.

166 To quantitatively validate changes in the brain activity in striatal subregions, we analyzed
167 the amount of ^{18}F-FDG uptake in the voxel of interest of these subregions (***Figure 2I***). The ^{18}F-
168 FDG uptake in the bilateral aDLS reached a peak on Day 6, and it decreased during the subsequent
169 days (***Figure 2J***), whereas the uptake in the bilateral pVLS gradually increased along with the
170 progress of learning, showing the maximal value on Day 10 (***Figure 2K***). The uptake in the DMS
171 did not alter during the acquisition phase, and it decreased on Day 24 (***Figure 2L***). These results
172 suggest that the aDLS and pVLS contribute to learning processes in a different temporal pattern
173 during the acquisition phase, whereas the DMS may be engaged to the behavior in the learned
174 phase.

175

176 **Excitotoxic lesion of the aDLS and pVLS, but not the DMS, disrupts the acquisition of**
177 **auditory discrimination**

178 To study whether the changed activity of striatal subregions is involved in learning processes, rats
179 received a bilateral injection of solution containing ibotenic acid (IBO; 8 mg/mL, 0.3 μL/site) or
180 phosphate buffered saline (PBS) into the subregions, and we conducted for the behavioral study.
181 The range of IBO lesion in the subregions was analyzed by immunostaining with a neuronal marker
182 NeuN after the behavioral tests (***Figure 3A–C***). The number of single lever presses increased
183 similarly along with the training in both the PBS- and IBO-injected groups into the aDLS, pVLS, or
184 DMS along with the training (***Figure 3D–F***). For the aDLS injections, increases in success rate
185 were impaired during the acquisition phase in the IBO group, compared to the PBS group, and the
186 impairments were mainly observed at the middle stage (***Figure 3G***). For the pVLS injection,
187 success rate impairments were observed in the IBO group showed compared to the PBS group,
188 although the period showing a significant difference was unclear (***Figure 3H***). The response time in

189 the aDLS-lesioned group did not alter during the discrimination training, whereas that in the pVLS-
190 lesioned group was continuously prolonged (***Figure 3–figure supplement 1A and B***), and the
191 omission rate and response bias were similar between the lesioned and the corresponding control
192 groups (***Figure 3–figure supplement 1D and G*** for aDLS lesion, and ***Figure 3–figure supplement***
193 ***1E and H*** for pVLS lesion). In contrast, for the DMS injection the success rate in the discrimination
194 task was comparable between the PBS and IBO groups (***Figure 3I***). The DMS lesion lengthened
195 the response time through the learning (***Figure 3–figure supplement 1C***), whereas it did not alter
196 the omission rate and response bias (***Figure 3–figure supplement 1F and I***). These results indicate
197 that the aDLS and pVLS are necessary for the acquisition of auditory discrimination, and that the
198 aDLS appears to be mainly involved in the learning process at the middle stage. The results also
199 reveal that the DMS contributes to the execution, but not learning, of discriminative behavior.
200 Previous studies have reported that the dorsal striatum is involved in both behavioral
201 strategies based on the stimulus-response association and the response-outcome association and
202 during instrumental learning (***Dickinson, 1985; O'Hare et al., 2016***). To assess the impact of
203 striatal lesions on the behavioral strategies, we analyzed the proportions of responses attributed to
204 two strategies in all responses of each session. One is the "win-shift-win" strategy, which is
205 considered to reflect the behavioral strategy based on the stimulus-response association (***Bergstrom***
206 ***et al., 2018; Packard et al., 1989***). In this strategy, after a correct response in the previous trial, the
207 rats press the opposite lever in the current trial in response to a shift of the instruction cue, resulting
208 in the correct response. Another strategy is the "lose-shift-lose" strategy, which is considered to
209 appear as a consequence of the behavioral strategy based on the response-outcome association
210 (***Bergstrom et al., 2018***). In this strategy, after an error response in the previous trial, the rats press
211 the opposite lever in the current trial, despite a shift of the instruction cue, leading to another error
212 response. In the control group into either of three striatal subregions, the proportions of win-shift-
213 win and lose-shift-lose strategies increased and decreased, respectively, during the acquisition phase
214 (***Figure 3J–L***). The changes in the proportion of the two strategies were similar to those in the

intact rats (***Figure 1–figure supplement 1***). For the aDLS injection, the increases in the win-shift-win proportion were markedly impaired in the IBO group compared to the PBS group with significant differences mainly at the middle stage, and the decrease in the lose-shift-lose proportion was delayed compared to the same group (***Figure 3J***). For the pVLS-injection, the increasing win-shift-win proportion was also impaired in the IBO group compared to the PBS group, although the change in the lose-shift-lose proportion was comparable between the two groups (***Figure 3K***). In contrast, for the DMS lesion both win-shift-win and lose-shift-lose proportions in the IBO group did not show significant differences from the corresponding values in their control group (***Figure 3L***). These results indicate that the aDLS promotes the win-shift-win strategy through stimulus-response association and suppresses the lose-shift-lose strategy rooted in response-outcome association, and that the pVLS selectively facilitates the win-shift-win strategy acquisition. Thus, these two subregions not only play roles in the acquisition of auditory discrimination but also control distinct behavioral strategies during the learning processes.

After the completion of discrimination training, we tested feeding behavior and locomotion of rats with aDLS and pVLS lesions. There was no difference in the amount of food intake and locomotor activity in the open field in both lesioned groups (***Figure 3–figure supplement 2A-D***), suggesting that learning deficits following excitotoxic lesions of the striatal subregions cannot be attributable to abnormalities in these general motor behaviors.

Inhibiting aDLS and pVLS activity impairs discriminative behavior at different stages of the acquisition phase

Our ^{18}F-FDG-PET imaging study indicated that the brain activity in the aDLS and pVLS was increased in a different temporal pattern during the acquisition phase of auditory discrimination. To examine whether neuronal activity in striatal subregions is linked with the processes at different stages, we temporarily inhibited the activity in each subregion by the treatment with a $GABA_A$ receptor agonist muscimol (MUS). In a pilot study, we tested the effect of the bilateral injection of

241 several doses of MUS (0.1, 0.2, and 0.5 μg/μL) into the aDLS or pVLS on the single lever press
242 behavior and confirmed that the administration of the lowest dose of MUS did not change the
243 frequency of single lever presses as compared to the saline (SAL) injection (***Figure 4–figure***
244 ***supplement 1A and B***). The lowest dose of MUS into the two striatal subregions unaffected the
245 amount of food intake (***Figure 4–figure supplement 1C and D***). In addition, to achieve the stage-
246 specific inactivation of the aDLS or pVLS neurons, rats were given bilateral injections of MUS (0.1
247 μg/μL, 0.25 μL per site) or SAL at three different timings during a series of the training. The first
248 injection was conducted on Day 2 to target the early stage. The second and third injections were
249 conducted on the day after the success rate had reached 60% and 80% for the first time through the
250 training, respectively, to target the middle or late stage. After the injections, the rats were used for
251 the behavioral test. Placement locations of the injection cannula into the striatal subregions were
252 assessed by cresyl violet staining after the behavioral tests (***Figure 4A and B***). The success rates on
253 the day before the injection (Day N-1) at the early, middle, and late stages were similar between the
254 two groups that received the bilateral injections of MUS or SAL (***Figure 4–figure supplement 2A***
255 ***and B***). Rats were then administered injections into the aDLS on the next day (Day N), and the
256 success rate in the MUS-injected groups significantly decreased at the middle stage compared to the
257 corresponding SAL-injected groups, but not at the early and late stages (***Figure 4C***, left). In
258 contrast, the success rate in the MUS groups into the pVLS significantly decreased at the late stage,
259 but not at the early and middle stages, compared with the respective SAL groups (***Figure 4D***, left).
260 To normalize the variation of learning speed in the individual animals, we calculated the value by
261 subtracting the success rate on Day N-1 from that on Day N in the individual animals. There were
262 significant reductions in the subtracted rate at the middle stage in the MUS-injected group into the
263 aDLS (***Figure 4C***, right) and at the late stage in the MUS-injected group into the pVLS (***Figure 4D***,
264 right). These results indicate that the aDLS and pVLS mainly function at the middle and late stages,
265 respectively, in the acquisition phase of auditory discrimination, supporting the results obtained
266 from our imaging study.

267 Next, we analyzed the influence of temporal striatal inactivation on the behavioral strategy
268 at the middle and late stages of the acquisition phase. We calculated the proportions of the win-
269 shift-win and lose-shift-lose strategies, and subtracted the values of these proportions on Day N-1
270 from those on Day N. The proportion of both strategies on Day N-1 were comparable between the
271 MUS- and SAL-injected groups (***Figure 4–figure supplement 3A and B***). In the aDLS, the
272 subtracted proportion of the lose-shift-lose strategy at the middle stage significantly increased in the
273 MUS group as compared to the SAL group, although the subtracted proportion of the win-shift-win
274 strategy tended to decrease in the MUS group as compared to the control group (***Figure 4E***), and
275 the subtracted proportions of the win-shift-win or lose-shift-lose strategy at the late stage was
276 similar between both groups (***Figure 4F***). In the pVLS, the subtracted proportions of the win-shift-
277 win and lose-shift-lose strategies at the middle stage were similar between the MUS and SAL
278 groups (***Figure 4G***), and the subtracted win-shift-win proportion at the late stage significantly
279 decreased in the MUS group as compared to the SAL group, although the subtracted lose-shift-lose
280 proportion was comparable between the two groups (***Figure 4H***). Our results show that transient
281 inhibition of aDLS activity at the middle stage affects the lose-shift-lose strategy and has a subtle
282 effect on the win-shift-win strategy, supporting that the aDLS mediates the acquisition process of
283 auditory discrimination at the middle stage at least partly through the suppression of the behavior
284 based on the response-outcome association. Although the impact of inhibition on the win-shift-win
285 strategy was subtle, excitotoxic lesion of the aDLS influenced the win-shift-win strategy in addition
286 to the lose-shift-lose strategy (see ***Figure 3J***), suggesting that the aDLS acts to enhance the auditory
287 discrimination by promoting the stimulus-response association, together with the suppression of the
288 response-outcome association. The discrepancy in the extent of changes in the win-shift-win
289 strategy between the two treatments may be generated from the difference in the timing or
290 sustainability of drug inhibition of the striatal subregion. In addition, our results show that pVLS
291 inactivation at the late stage selectively impairs the win-shift-win strategy, supporting contribution
292 of the pVLS to the process via progression of the stimulus-response association.

Neuronal activity in the aDLS and pVLS during the acquisition phase

To examine the firing activity in striatal subregions during the acquisition phase of auditory discrimination, we simultaneously recorded neuronal activity in the aDLS and pVLS at the unilateral (left) side by using a multi-unit recording procedure (***Figure 5A***). Using immunostaining for tyrosine hydroxylase (TH) after the recordings, we verified the location of electrodes within the striatal subregions (***Figure 5B***). After the single lever press task, we conducted the auditory discrimination task for the recordings. In correct trials, the delay period (0.5 ± 0.2 s) was inserted between a lever press and a sound indicating the reward to distinguish neuronal activity related to the two events (***Figure 5C***). The behavioral data in individual rats were divided into three grouped sessions corresponding to the early, middle, and late stages, based on a sigmoid function analysis (***Bathellier et al., 2013***) of the success rate in the task. The success rates in the grouped sessions were 52.7 ± 0.8 %, 61.6 ± 0.7 %, and 85.3 ± 1.7 % (mean ± s.e.m.) for the early, middle, and late stages, respectively, and the rate was significantly increased throughout the three stages (***Figure 5–figure supplement 1A***). However, the response time, omission rate, and response bias were similar among the stages (***Figure 5–figure supplement 1B-D***). Thus, these stages corresponded to the timing window defined in the acquisition phase of the transient MUS inhibition experiment of neuronal activity.

We identified 1,062 and 423 well-isolated neurons from the aDLS and pVLS, respectively, across the three stages (***Figure 5–figure supplement 2A***) and focused on the major population of striatal neurons, putative medium spiny neurons (MSNs; ***Figure 5–figure supplement 2B***). The numbers of MSNs were 96% and 91% of the total numbers of identified neurons in the aDLS and pVLS, respectively (***Figure 5-figure supplement 2C***). The neuron numbers at the early, middle, and late stages were 295, 364, and 360 neurons in the aDLS, and 87, 110, and 190 neurons in the pVLS, respectively. Based on the combinatorial pattern of the tone instruction cue and lever press in our discrimination task, we categorized the electrophysiological data into four trial types: (1) high-frequency tone/right lever press (HR) and (2) low-frequency tone/left lever press (LL) as correct

319 responses; and (3) high-frequency tone/left lever press (HL) and (4) low-frequency tone/right lever
320 press (LR) as error responses (see ***Figure 1A***). We identified HR or LL type neurons showing
321 significant changes in firing rate related to the cue onset, choice response, reward sound, or first
322 licking as compared to the baseline firing rate in each of two trials (Mann-Whitney *U* test, $p <$
323 0.01). These neurons were further divided into two groups based on increased or decreased activity
324 (***Figure 5–figure supplement 3A and B***). In the following analyses, we focused on the HR and LL
325 type neurons with increased event-related activity to explore the firing patterns of neurons
326 underlying behavioral processes of auditory discrimination.
327

328 **Subpopulations of aDLS neurons, but not of pVLS neurons, show firing activity related to the**
329 **behavioral outcome**

330 Previous studies have reported that neurons in the dorsal striatum show the outcome-related activity
331 in the instrumental conditioning tasks (***Guo et al., 2019; Nonomura et al., 2018***). We thus
332 investigated whether aDLS and pVLS neurons exhibit a response related to the behavioral outcome
333 during the acquisition of auditory discrimination. In the aDLS, the firing activity of reward sound-
334 related HR type neurons showed a higher extent in the increase during a period, when the reward
335 sound is presented in the correct responses, in the HR trial as compared with the LL, HL, or LR trial
336 throughout the three stages (***Figure 5D***, top rows). The rate of these neurons also moderately
337 increased during the same period in the LR trial compared to the LL or HL trial across the three
338 stages, although the extent of the increase was lower than that in the HR trial (***Figure 5D***, top
339 rows). The area under the receiver operating characteristic (auROC) values revealed a significant
340 difference of the HR trial from the LR trial during the reward sound period, whereas the values of
341 LL and HL trials indicated a significant difference from the LR trial in the opposite direction during
342 the same period (***Figure 5D***, bottom rows). The averaged firing rate during the reward sound period
343 in the HR or LR trial appeared to modestly increase at the middle stage, but no significant
344 difference existed among the stages (***Figure 5E***). To directly compare the number of neurons

345 showing event-related activity among different stages, we calculated the number of reward sound-
346 HR type neurons by matching the trial number at each stage (***Figure 5F***). The proportion decreased
347 progressively from the early to middle stages, and to the late stage. In addition, the firing rate of
348 reward sound-related LL type neurons exhibited a higher increase in the LL trial and a modest
349 increase in the HL trial while the averaged firing rate during the reward sound period was similar
350 among the three stages (***Figure 5–figure supplement 4A and B***). Furthermore, the proportion of
351 reward sound-LL neurons reduced progressively through the stages (***Figure 5–figure supplement***
352 ***4C***). These results indicate that the aDLS contained neurons related to the outcome of choice,
353 showing a greater increase in the firing activity for the correct responses (HR and LL trials) than the
354 error responses (HL and LR trials), and that the proportion of these subpopulations was gradually
355 reduced through the progress of learning. In contrast, during the reward sound period at all stages,
356 the firing rate and auROC values of reward sound-HR and reward sound-LL type neurons in the
357 pVLS revealed no significant differences across the four kinds of trial (***Figure 5–figure supplement***
358 ***5A and B***), indicating that the firing activity of pVLS neurons did not appear to be associated with
359 the behavioral outcome.
360

361 **Subpopulations of aDLS and pVLS neurons show sustained firing activity after the reward in**
362 **different manners**

363 The dorsal striatum is known to demonstrate a response of neuronal activity after the positive
364 outcome in the instrumental behaviors (***Smith and Graybiel, 2016; Williams and Eskandar, 2006***).
365 We thus examined whether aDLS and pVLS neurons show the response after obtaining the reward
366 during the acquisition phase of auditory discrimination. In the aDLS, the firing rate of the first
367 licking-related HR type neurons indicated a sustained elevation after the first licking in the HR trial
368 as compared with any of the other three trials across the early, middle, and late stages (***Figure 6A***,
369 top rows). The auROC values revealed a significant difference of the LL, HL, or LR trial from the
370 HR trial across the three stages (***Figure 6A***, middle rows). In addition, we calculated the averaged

371 firing rate and increased firing period, defined as the total number of time bins above 3 s.d. of the
372 baseline firing rate for 5 s after the first licking in the HR trial. The averaged firing rate was
373 comparable between the early and middle stages, but the rate was significantly lower at the late
374 stage compared to either of the other two stages (***Figure 6B***). The increased firing period was also
375 comparable between the early and middle stages, showing a significant reduction at the late stage
376 (***Figure 6C***). The proportions of first licking-HR type neurons were similar between the early and
377 late stages, although they showed a slight decrease at the middle stage (***Figure 6D***). There were
378 only a few neurons with significant correlations between the firing rate and licking performance
379 (***Figure 6E***). In addition, the firing rate of the first licking-related LL type neurons exhibited the
380 largest increase in the LL trial at the three stages, showing a tendency to reduce the average firing
381 rate and increased firing period after the first licking across the stages (***Figure 6–figure supplement***
382 ***1A-C***). The proportion of first licking-LL type neurons during the learning processes displayed
383 similar changes as observed in the first licking-HR neurons, and there were few neurons with
384 significant correlations between the firing rate and licking performance (***Figure 6–figure***
385 ***supplement 1D and E***). These results indicate that the aDLS contained neurons showing long-
386 lasting, increased activity after the reward in the specific correct combination of the stimulus and
387 response (HR or LL trial), and that the extent of firing activity and length of firing period in the
388 response appeared to be gradually reduced with no correlation between the proportion of neurons
389 and the progress of the learning stages.

390 In the pVLS, the first licking-HR type neurons showed a sustained elevation in the firing
391 rate after receiving a reward in the HR trial compared to that in the HL or LR trial throughout the
392 three stages (***Figure 6F***, top rows). A similar elevation in the firing rate was also observed in the LL
393 trial throughout the stages (***Figure 6F***, top rows). The auROC values revealed a significant
394 difference of the HL or LR trial, but not the LL trial, from the HR trial throughout the stages
395 (***Figure 6F***, middle rows). The average firing rate did not show significant changes among the three
396 stages (***Figure 6G***), and the increased firing period was also similar across the stages (***Figure 6H***).

397 The proportion of first licking-HR neurons increased at the late stage compared to the early or
398 middle stage (***Figure 6I***). The firing rate showed almost no significant correlation to the licking
399 performance (***Figure 6J***). In addition, the first licking-LL neurons exhibited similar firing patterns
400 and changes in the proportion of neurons across the stages (***Figure 6–figure supplement 2A-E***).
401 Therefore, the pVLS included neurons representing the long-lasting increased activity after the
402 reward in the two kinds of correct responses (HR and LL trials) with the increased number of these
403 neurons at the late stage of learning.
404
405 **Neurons in the pVLS, but not in the aDLS, exhibit firing patterns related to the beginning and**
406 **ending of the behavior**
407 The dorsal striatum plays a key role in the acquisition and execution of behaviors based on the
408 stimulus-response association, and the association is accompanied by a transient activation of
409 neuronal firing immediately after the stimulus presentation or action in trials, which is considered to
410 represent the beginning and ending of a learned behavior (***Barnes et al., 2005; Jin and Costa,***
411 ***2010; Jog et al., 1999***). We first examined whether the firing activity of cue onset-related HR and
412 LL type neurons corresponds to the beginning of the behavior in the auditory discrimination task. In
413 the aDLS, the firing rate of both types of neurons showed a significant difference at some time
414 points in each trial compared to those in any of the other three trials, with a significant difference of
415 auROC values between the trials (***Figure 7–figure supplement 1A and B***). However, the transiently
416 increased activity did not emerge at the time points corresponding to the beginning of the behavior.
417 In contrast, the cue onset-related HR type neurons in the pVLS showed a transient increase in the
418 firing rate immediately after the cue onset, and the activity appeared at the middle and late stages
419 (***Figure 7A***, top rows). The transient activation was observed not only in the HR trial but also in the
420 other three trials, being consistent with the results of a previous report (***Barnes et al., 2011***). The
421 increased firing rate showed a slight but notable difference between the HR and LL trials with a
422 significant difference in the auROC values between the two kinds of trials (***Figure 7A***, bottom

423 rows), suggesting that different combinations between the stimulus and response may affect the
424 level of firing activity. The rate differences between the two trials were observed at the middle and
425 late stages (***Figure 7B***). The proportion of cue onset-HR neurons increased at the middle and late
426 stages compared to the early stage (***Figure 7C***). In addition, the firing rate of the cue onset-related
427 LL type neurons exhibited patterns similar to those observed in the cue onset-HR neurons (***Figure***
428 ***7–figure supplement 2A***). The data indicate that subpopulations of pVLS neurons show firing
429 activity related to the beginning of the behavior, with a rising number of neurons throughout
430 discrimination learning.

431 Next, we examined the firing activity of choice response-related HR and LL type neurons,
432 corresponding to the ending of a behavior in auditory discrimination. In the aDLS, the firing rate of
433 these neurons did not exhibit the transient increase related to the ending of the behavior, instead,
434 there was a modest increase before the lever press (***Figure 7–figure supplement 3A and B***). In
435 contrast, the choice response-related HR type neurons in the pVLS were transiently activated
436 immediately after the lever press in the four kinds of trial at the middle and late stages, and the rate
437 appeared to gradually decline toward the reward sound presentation (***Figure 7D***). The averaged
438 firing rate was similar between the HR and LL trials though the stages (***Figure 7E***). The proportion
439 of the choice response-HR neurons increased at the middle and late stages compared to the early
440 stage (***Figure 7F***). In addition, the rate of choice response-related LL type neurons displayed
441 similar firing patterns to those observed in the choice response-HR neurons (***Figure 7–figure***
442 ***supplement 2B***). Thus, subpopulations of pVLS neurons also represent the activity related to the
443 ending of the behavior in auditory discrimination, increasing the neuron number throughout the
444 learning stages in a similar pattern to neurons relevant to the beginning of the behavior in the task.
445

446 **Structure of neural circuits linked to the aDLS and pVLS**

447 Anatomically, striatal subregions are known to form heterogeneous cortico-basal ganglia loops in
448 mice (***Foster et al., 2021; Hintiryan et al., 2016; Hunnicutt et al., 2016***). To characterize the

449 structure of neural circuits connected to the aDLS and pVLS in rats, a solution containing cholera
450 toxin subunit B (CTb) labeled with Alexa 488 or Alexa 555 (1.0 mg/mL, 0.3 μL/site) as a
451 bidirectional tracer (***Amita et al., 2019***) was injected into the aDLS and pVLS of the same animals,
452 respectively (***Figure 8A***). Brain sections were prepared, and cell bodies and axon terminals were
453 detected by CTb with florescence signals. Sections through the aDLS and pVLS indicated the
454 florescence signals around the injection sites (***Figure 8B***). Alexa 488 signals were localized in cell
455 bodies in the bilateral, rostrodorsal regions of some cortical areas, including the primary motor
456 cortex, secondary motor cortex, primary somatosensory cortex, and secondary somatosensory
457 cortex, and in the ipsilateral regions of various thalamic nuclei, such as the centrolateral nucleus,
458 centromedian nucleus, parafascicular nucleus, and ventromedial nucleus, whereas Alexa 555 signals
459 were observed in the bilateral, ventrolateral regions of some cortical areas, including the most
460 rostral parts of the primary motor cortex, agranular/dysgranular/granular insular cortices, rhinal
461 cortex, and amygdala nucleus, as well as in the ipsilateral regions of various thalamic nuclei, such
462 as the centromedian nucleus, parafascicular nucleus, and medial geniculate nucleus (***Figure 8C and***
463 ***D***). In addition, Alexa 488 signals were distributed in axon terminals in the anterior part of the
464 globus pallidus (GP) and entopeduncular nucleus (EPN), whereas Alexa 555 signals were detected
465 in the posterior GP (***Figure 8E***). In the ventral midbrain. Alexa 488 and 555 signals in the nerve
466 terminals were distributed distinctively in the ventromedial and dorsolateral parts of the substantia
467 nigra pars reticulata (SNr), respectively, along with the rostrocaudal axis (***Figure 8F***). In the cell
468 bodies, both signals were localized in the centromedial and lateral parts of the substantia nigra pars
469 compacta (SNc), respectively (***Figure 8F***). The signals in the SNc were colocalized with
470 immunoreactivities for TH, a marker of dopamine neurons in the ventral midbrain (***Figure 8G***).
471 These results indicate that the aDLS and pVLS receive innervations from different subregions in the
472 cerebral cortex, intralaminar thalamus, and SNc, and send projections to different subregions in the
473 basal ganglia nuclei including the GP, EPN, and SNr, being consistent with previous anatomical

474 studies of cortico-basal ganglia loops (***Foster et al., 2021; Hintiryan et al., 2016; Hunnicutt et al.,***
475 ***2016***).
476

477 ## Discussion

478 Our findings demonstrate that the aDLS and pVLS are required for the acquisition of auditory
479 discrimination at different stages of learning, and that the DMS is not necessary for the acquisition
480 of discrimination, although it appears to contribute to the execution of actions, in particular to the
481 regulation of response time. These results not only support some recent studies reporting no
482 requirement of the DMS in the procedural learning (***Featherstone and McDonald, 2004; Smith et***
483 ***al., 2021; Wolff et al., 2022***), but also reveal important roles of two different subregions in the
484 lateral striatum in the external cue-dependent decision-making. We propose that aDLS and pVLS
485 neurons act to integrate the new learning of auditory discrimination in spatiotemporally and
486 functionally distinct manners, showing a remarkable difference from the prior learning model that
487 proposes the functional dominance changes from the DMS to DLS subregions during procedural
488 learning (***Dickinson, 1985; O'Hare et al., 2016; Redgrave et al., 2010; Yin et al., 2004: Yin et al.,***
489 ***2005***).

490 Our ^{18}F-FDG-PET imaging study demonstrated that the brain activity in the aDLS reaches
491 a peak at the middle stage of the acquisition phase of auditory discrimination (***Figure 2J***). The
492 results of excitotoxic lesion experiment of striatal subregions suggest that the aDLS functions to
493 enhance the acquisition of discrimination through the promotion of behavior based on the stimulus-
494 response association and the suppression of behavior based on the response-outcome association
495 (***Figure 3G and J***). Transient inhibition experiment of neuronal activity confirmed this aDLS
496 function at the middle stage of the learning, although the drug inhibition tended to reduce the
497 stimulus-response behavior (***Figure 4C, E and F***). In addition, we found subpopulations of aDLS
498 neurons (reward sound-related neurons) which represent the behavioral outcome and differentiate
499 the correct (HR or LL) and incorrect (HL or LR) choices (***Figure 5D*** and ***Figure 5–figure***

500 ***supplement 4A***). The distinct responses of these neurons may explain the mechanism by which the
501 aDLS regulates the stimulus-response and response-outcome associations through distinct neural
502 circuits leading to a differential control of the two associations. Alternatively, the responses mainly
503 promote the behavior based on the stimulus-response association, thereby secondarily inhibiting the
504 response-outcome association. Indeed, some previous studies have suggested that an action based
505 on either the stimulus-response association or response-outcome association is generated as a result
506 of competition between different striatal subregions (***Gremel et al., 2016***). We also found other
507 subpopulations of aDLS neurons (first licking-related neurons) showing long-lasting increased
508 activity after obtaining reward in response to a specific combination between the stimulus and
509 response (HR or LL trial) (***Figures 6A*** and ***Figure 6–figure supplement 1A***). This activity may
510 function as the feedback signal to promote the stimulus and response association, resulting in the
511 enhancement of discrimination learning. The proportion of neurons related to the behavioral
512 outcome showed a gradual reduction through the progress of auditory discrimination (***Figures 5F***
513 and ***Figure 5–figure supplement 4C***, and the extent of the firing activity and the length of the firing
514 period of neurons showing sustained activation after reward were also decreased at the late stage of
515 learning (***Figure 6B and C***). The learning-dependent changes in the properties of these
516 subpopulations in the aDLS may explain the mechanism underlying the earlier acquisition process
517 of the auditory discrimination.

518 The ^{18}F-FDG-PET imaging indicated that the pVLS activity was gradually elevated
519 through the acquisition phase of auditory discrimination, showing the maximal value at the late
520 stage (***Figure 2K***). The lesion experiment suggested that the pVLS drives the formation of
521 discrimination learning via the selective progression of the stimulus-response association (***Figure***
522 ***3H and K***), and the transient inhibition experiment ascertained the pVLS function at the late stage
523 of learning (***Figure 4D, G and H***). Previous studies have shown that the stimulus-response
524 association is encoded in the DLS or VLS as the transient neuronal activity representing the
525 beginning and ending of a learned behavior (***Barnes et al., 2005; Chen et al., 2021; Jin and Costa,***

526 ***2010; Jog et al., 1999***). A recent study reported that the VLS is causally related to learned
527 performance based on the auditory stimulus, while the DLS shows a weaker relationship to the
528 behavior (***Lee et al., 2020***). In the present study, we found subpopulations of pVLS neurons that
529 represent the beginning and ending of a behavior (cue onset- and choice response-related neurons,
530 respectively) (***Figure 7A and D***, ***Figure 7–figure supplement 2A and B***), showing an increased
531 number of neurons along with the progress of discrimination learning (***Figure 7C and F***). These
532 data suggest that pVLS neurons contribute to the formation of the stimulus-response association
533 through the learning processes. In addition, we found another subpopulation of pVLS neurons (first
534 licking-related neurons) that are continuously activated after the reward outcome in response to two
535 kinds of correct choices (HR and LL trials) (***Figure 6F*** and ***Figure 6–figure supplement 2A***), and
536 the proportion of neurons was increased at the late stage (***Figure 6I*** and ***Figure 6–figure***
537 ***supplement 2D***). This activity may act as a feedback signal to consolidate the stimulus and response
538 association, leading to the maintenance of associative memory at the late stage during the
539 acquisition phase of learning.

540 In the present study, we identified neurons with four kinds of event-related activity in the
541 aDLS and pVLS, and classified them into the HR and LL type neurons (***Figure 5-7***, ***Figure 5-***
542 ***figure supplement 4 and 5***, ***Figure 6-figure supplement 1 and 2***, and ***Figure 7-figure supplement***
543 ***1-3***). Parts of these two types of neurons with the respective event-related activity overlapped, and
544 the numbers of overlapping neurons varied between striatal subregions. In the pVLS, the
545 overlapping neurons for the same event-related activities were 35.1%, 45.2%, and 67.0% in the cue
546 onset, choice response, and first licking, respectively. In contrast, the aDLS had lower overlaps of
547 12.6% and 22.7% in the reward sound and first licking, respectively. Thus, distinct neurons in the
548 aDLS tend to have properties of a single trial type while the same neurons in the pVLS seem to
549 possess properties of both types. One possible explanation for the diversity in the proportion of
550 overlapping neurons between the two subregions may be the difference of input patterns into striatal
551 neurons or plastic changes in functional connectivity during learning processes. The detailed

552 mechanism by which aDLS and pVLS neurons react to the events in a different manner should be
553 investigated in the future.
554 We examined the neural circuits linked to the aDLS and pVLS in rats by using
555 bidirectional tracers. The results showed that these two striatal subregions receive innervations from
556 different subregions in the cerebral cortex, intralaminar thalamus, and ventral midbrain, and provide
557 projections to different subregions in the basal ganglia nuclei (***Figure 8***), confirming that the two
558 subregions form the heterogenous cortico-basal ganglia loops in the rodent brain (***Foster et al.,***
559 ***2021; Hintiryan et al., 2016; Hunnicutt et al., 2016***). These data suggest that the aDLS and pVLS
560 mediate the acquisition of auditory discrimination via the parallel loops, and cooperate to achieve
561 neural processing related to the dual regulation of the stimulus-response and response-outcome
562 associations. Further studies are needed to elucidate the mechanism by which the two kinds of loops
563 are processed separately and integrate the new learning of discrimination.
564

565 **Limitations**

566 In the ^{18}F-FDG PET neuroimaging study, the brain activity in the aDLS reached a peak at the
567 middle stage of the acquisition phase of auditory discrimination (***Figure 2J***). In the multi-unit
568 electrophysiological recording experiment, the firing activity of aDLS neuron subpopulations
569 related to the behavioral outcome showed no significant differences among the three stages (***Figure***
570 ***5E*** and ***Figure 5-figure supplement 4B***), while the proportions of these subpopulations gradually
571 reduced through the progress of learning stages (***Figure 5F*** and ***Figure 5-figure supplement 4C***).
572 The extent of firing activity and length of firing period of other subpopulations showing sustained
573 activation after the reward appeared to show learning-dependent decrease (***Figure 6B and C***, and
574 ***Figure 6-figure supplement 1B and C***), although the proportions of these subpopulations indicated
575 no correlation to the progress of the learning (***Figure 6D*** and ***Figure 6-figure supplements 1D***).
576 The patterns of the temporal changes in the brain activity of the striatal subregions during the
577 learning stages did not match completely the time variation in the property and proportion of

578 specific event-related neurons. In our electrophysiological analysis, we identified well-isolated
579 neurons from striatal subregions across the behavioral task, focusing on putative MSNs (***Figure 5–***
580 ***figure supplement 2***). Based on the combinatorial pattern of the tone instruction cue and lever
581 press, we categorized the electrophysiological data into the four trials, including the HR, LL, HL,
582 and LR. We identified HR or LL type neurons showing significant changes in the firing rate related
583 to specific events compared to the baseline firing rate. These neurons were further divided into two
584 groups with increased or decreased activity relative to the baseline firing (***Figure 5–figure***
585 ***supplement 3***). In the present study, we focused on event-related neurons with the increased
586 activity. Because the analysis was limited to neuronal subpopulations related to specific events with
587 the increased activity, we consider that it is difficult to explain fully dynamic shifts in the brain
588 activity of the striatal subregions dependent on the progress of learning by the time variation of
589 firing activity of individual event-related neurons. The activity of other subpopulations in the
590 striatum may be involved in the shifts in brain activity during the learning processes. In addition,
591 recent studies have reported that the activity of glial cells influences the uptake of ^{18}F-FDG and that
592 these cells regulate spike timing-dependent plasticity (***Valtcheva and Venance, 2016***). Changes in
593 glial cellular activity, through the control of synaptic plasticity, may partly contribute to the pattern
594 formation of learning-dependent shift of brain activity.
595

596 ## Materials and Methods

Key Resources Table

Reagent type (species) or resource	Designation	Source or reference	Identifiers	Additional information
Strain, strain background (*Rattus norvegicus,* Long-Evans)	Long-Evans Rats	Institute for Animal Reproduction		Wild-type rats

Antibody	Donkey anti-mouse IgG antibody conjugated with Alexa Fluor 647 (polyclonal)	Thermo Fisher Scientific	Cat# A-31571; RRID:AB_162542	1:1,000
Antibody	Goat anti-mouse IgG antibody conjugated with Alexa Fluor 488 (polyclonal)	Jackson Immunoreseach Laboratories	Cat# 715-545-151; RRID:AB_2341099	1:1,000
Antibody	Mouse anti-NeuN antibody (monoclonal)	Millipore	Cat# MAB377; RRID:AB_2298772	1:1,000
Antibody	Mouse anti-TH antibody (monoclonal)	Millipore	Cat# MAB318-AF488; RRID:AB_2201528	1:1,000
Chemical compound, drug	(±)-Ibotenic acid	FUJIFILM Wako Pure Chemical	Cat# 533-54971	0.8 mg/mL
Chemical compound, drug	Muscimol	Sigma-Aldrich	Cat# M1523	0.1 µg/µL
Chemical compound, drug	Saccharin sodium salt dihydrate	Tokyo Chemical Industry	Cat# B0131	0.02%
Software, algorithm	Kilosort2	Marius Pachitariu ***Stringer et al., 2015***	RRID: SCR_016422	https://www.github.com/MouseLand/Kilosort2
Software, algorithm	KlustaKwik2	***Kadir et al., 2014***	RRID: SCR_014480	https://github.com/kwikteam/klustakwik2
Software, algorithm	MATLAB	MathWorks	RRID: SCR_001622	

Software, algorithm	phy	cortex-lab	RRID: SCR_016249	https://github.com/cortex-lab/phy
Software, algorithm	PMOD version 3.2	PMOD Technologies	RRID: SCR_016547	https://www.pmod.com/web/
Software, algorithm	SPM version 8	Wellcome Department of Imaging Neuro science	RRID:SCR_007037	https://www.fil.ion.ucl.ac.uk/spm/
Software, algorithm	SPSS version 27	IBM	RRID: SCR_002865	
Other	Cholera toxin subunit B conjugated to Alexa 488	Invitrogen	Cat# C34775; RRID: AB_2536189	1.0 mg/mL
Other	Cholera toxin subunit B conjugated to Alexa 555	Invitrogen	Cat# C34776; RRID: AB_968419	1.0 mg/mL
Other	Cresyl violet	Muto Pure Chemicals	Cat# 41021	0.1%
Other	DAPI	Thermo Fisher Scientific	Cat# D1306; RRID: AB_2629482	0.1 µg/mL
Other	DAPI and red fluorescent Nissl stain solution	Thermo Fisher Scientific	Cat# N21482; RRID:AB_2620170	1:10,000/ 1:200
Other	Grain-based precision pellets	Bio-serv	Cat# F0021	45 mg
Other	Guide cannula	P1 Technologies	Cat# C315I	26 gauge
Other	Internal cannula	P1 Technologies	Cat# C315G	30 gauge
Other	Laboratory chow	CLEA Japan	Cat# CE-2	
Other	Silicon probe	NeuroNexus	Buzsaki64spL	64-channel (6-shank)

Other	Templates for the Long-Evans rat brain	Neuroimaging Tools and Resources Collaboratory	RRID:SCR_003430	https://www.nitrc.org/projects/tpm_rat/
Other	Thin wall borosilicate glass	Sutter Instrument	Cat# B100-75-10	60-µm diameter

597

598 **Animals**

599 Animal care and handling procedures were carried out in accordance with the guidelines established
600 by RIKEN Center for Biosystems Dynamics Research, Fukushima Medical University, and Osaka
601 City University. All procedures were approved by their Institutional Animal Care and Use
602 Committees. All efforts were made to minimize the number of animals used and their suffering
603 throughout the course of the experiments. Male Long-Evans rats (8–13 weeks old, Institute for
604 Animal Reproduction, Ibaraki, Japan) were used for the present study. The rats were kept at 22 ±
605 2 °C and 60% humidity in a 12-h light/12-h dark cycle, and were continuously available for
606 laboratory chow (CE-2, CLEA Japan, Fukuoka, Japan) and water. Three days before the behavioral
607 training, the rats were subjected to dietary restriction to maintain their body weight at ~85% of the
608 free feeding weight or water restriction in which they received free access to water for 6 to 9 h each
609 day.

610

611 **Surgery**

612 Rats underwent a stereotaxic surgery under isoflurane anesthesia (1–5%). For excitotoxic lesion of
613 striatal neurons, a solution containing IBO (533-54971, FUJIFILM Wako Pure Chemical, Osaka,
614 Japan) in PBS (0.8 mg/mL, 0.3 µL per site) was injected bilaterally with the coordinates (mm) from
615 bregma and dura for the aDLS (AP +1.6, ML ±3.3, DV -3.9), pVLS (AP -1.6, ML ±4.6, and DV -
616 5.6), or DMS (AP -1.6, ML ±1.4, and DV -4.8) according to the atlas of rat brain (***Paxinos and***
617 ***Watson, 1998***). Injection was performed through a thin-wall borosilicate glass pipette (diameter: 60
618 µm, B100-75-10, Sutter Instrument, Novato, CA) at a constant velocity of 0.1 mL/min with the

619 microinfusion pump (ESP-32, EICOM, Kyoto, Japan). For transient inactivation of striatal neurons,
620 two guide cannulae (length: 10 mm, outer diameter: 26 gauge, C315G, P1 Technologies, Roanoke,
621 VA) were bilaterally placed on the skull and fixed using four screws and dental cement. The chip of
622 the cannula was placed at 1 mm above the target coordinates. A solution containing MUS (M1523,
623 Sigma-Aldrich, St. Louis, MO) in saline (0.1 μg/μL, 0.25 μL per site) was injected into the target
624 coordinates through the internal cannula (outer diameter: 30 gauge, C315I, P1 Technologies) at a
625 constant velocity of 0.25 μL/min. For the electrophysiological experiments, surgery was performed
626 as described previously (***Kitanishi et al., 2021***). A 64-channel silicon probe (Buzsaki64spl,
627 NeuroNexus, Ann Arbor, MI) attaching to a 3D-printed microdrive with a movable screw was
628 chronically implanted with the coordinates (mm) from the bregma and dura into the left aDLS (AP
629 +1.6, ML -3.3, and DV -2.5) and pVLS (AP -1.6, ML -4.6, and DV -3.6). A faraday cage composed
630 of copper mesh was secured on the skull with dental cement to reduce electrical noise and avoid
631 damage to the implants. For anterograde and retrograde tracing, a solution containing CTb
632 conjugated to Alexa 488 (1.0 mg/mL, C34775, Invitrogen, Waltham, MA) or CTb conjugated to
633 Alexa 555 (1.0 mg/mL, C34776, Invitrogen) was injected into the aDLS and pVLS (0.3 μL/site),
634 respectively. The coordinates for the injection into striatal subregions were the same as described
635 above. The rats were allowed to recover for 1 week after the surgeries.
636
637 **Behavioral analysis**
638 The behavioral tasks were conducted in operant conditioning chambers (30.5 × 24.1 × 29.2 cm;
639 ENV-007, MED Associates, Fairfax, VT) equipped with two retractable levers on both sides of a
640 reward port in the front panel (ENV-203M-45, ENV-112CM, and ENV-201A, MED Associates). A
641 multi-tone generator (ENV-223, MED Associates) and room light were mounted on the top of the
642 center and corner panels on the rear side, respectively. For the electrophysiological experiment, a
643 3D printed reward port was used to detect the licking and to prevent contact with the head
644 attachment and front panel. The behavioral experiment was performed using reinforcement pellets

645 (grain-based precision pellets; F0021, Bio-serv, Flemington, NJ) as a food reward. To prevent
646 spillover of radioactivity into the temporal cortex as a consequence of excessive ^{18}F-FDG
647 accumulation into the muscles by their activity to eat the pellets (***Endepols et al., 2010; Marx et al.,***
648 ***2012***). the PET imaging experiment was carried out using 0.02% saccharin solution (B0131, Tokyo
649 Chemical Industry, Tokyo, Japan) as a liquid reward. The electrophysiological experiment was also
650 carried out by using the saccharin solution.
651 The training schedule consisted of four continuous steps. In the first step (magazine
652 training), rats were habituated to the operant conditioning chambers, and the reward was presented
653 with the click every 20 s. Each daily session was started by illumination of the room light, and
654 continued for 30 min. The sessions were conducted for 3 consecutive days. In the second step
655 (shaping), only one lever on the left or right side was inserted. When the rats pressed the lever, they
656 earned a reward accompanied by a click. Each daily session was started by illumination of the light,
657 and lasted 30 min or until the criteria, in which the rats received 90 rewards. When the number of
658 lever presses on either side reached the criteria, the lever was inserted in the opposite side on the
659 next day. When the rats achieved the criteria on both sides for 2 or 3 days, they moved to the
660 following step. In the third step (single lever press task), each trial was started by illumination of the
661 light and insertion of one lever on either the left or right side in a pseudorandom manner with equal
662 frequencies on both sides for every set of four trials. When the rats pressed the lever, the reward
663 was presented with the sound, and the lever was immediately retracted. The room light turned off 4
664 s after the lever press. When they did not press the lever within 10 s after the start, the trial was
665 terminated when the light turned off. The trial was repeated every 20 s. Each daily session
666 continued for 30 min, and the sessions were conducted for 4 consecutive days. The number of lever
667 presses in each session was counted. In the final step (two-alternative auditory discrimination task),
668 each trial was started by the presentation of a high (10 kHz) or low (2 kHz) frequency tone as an
669 instruction cue in a pseudorandom manner. After 3 s, the room light was illuminated, and two
670 retractable levers were inserted at the same time. The rats were required to press the left or right

levers in response to the low or high tone cues, respectively. When the rats pressed the correct lever, the reward was presented with the sound, and the levers were immediately retracted. Correct response allowed the rats to access the reward: the retractable spout delivering water was inserted for 1 s for the PET imaging experiment; a pellet was delivered by a food dispenser for the pharmacological experiment; and three drops of water were delivered through a solenoid valve for the electrophysiological experiment. The room light turned off 4 s after the correct response. On the other hand, error response resulted in the retraction of levers and the turning off of the room light. No response within 10 s after the lever insertion was recorded as an omission response. The success rate in each session was calculated by dividing the number of correct response trials with the number of lever press trials minus the number of omission trials. The trial was repeated every 20 s. Each daily session continued for 60 min, and the sessions were conducted for 14 or 24 days according to the experiments.

To assess the behavioral strategies in the auditory discrimination task, a trial-by-trial analysis was conducted; the win-shift-win strategy was defined as a correct response, in which, after a correct response during the previous trial, the rats press the opposite lever during the current trial in response to the shift of the tone instruction cue; the lose-shift-lose strategy was defined as an error response, in which, after an error response during the previous trial, the rats press the opposite lever during the current trial despite the shift of the instruction cue. The proportion of both strategies was calculated by dividing the number of each strategy with the number of lever press trials minus the number of omission trials.

For the transient inactivation experiment, MUS injections were bilaterally performed 20 min before start of the session. For habituation, all rats were injected with saline bilaterally into the corresponding striatal subregions on the last day (Day 4) of the single lever press task. During the auditory discrimination task, the first injection was conducted on Day 2 of the task. The second and third injections were conducted the next day, after the success rate had exceeded 60% and 80%, respectively. Each session continued for 15 min.

697 For the electrophysiological experiments, a delay period (0.5 ± 0.2 s) was added in the
698 auditory discrimination task between the lever press and reward sound to distinguish the motor- and
699 reward-related responses of neurons. When the rats pressed the lever, it was immediately retracted.
700 After the delay period, the reward was presented with a sound. The room light turned off 4 s after
701 the lever press. The trial was repeated every 20 s, and each daily session continued for 60 min.
702

703 **PET imaging analysis**

704 An ^{18}F-FDG-PET scan was performed with a microPET Focus220 (Siemens Medical Solutions,
705 Knoxville, TN) designed for high-resolution imaging of small animals (spatial resolution of 1.4 mm
706 in full width at half maximum at the center of the field of view) as described previously (***Cui et al.,***
707 ***2015***). Serial ^{18}F-FDG-PET scans were performed on the last day of the single lever press task and
708 on Days 2, 6, 10, and 24 of auditory discrimination task. To administer ^{18}F-FDG under the awake
709 condition, rats were anesthetized through an indwelling catheter attached to their tail with 5%
710 induction and 2.0–2.5% maintenance of isoflurane (median [interquartile range]: 6 [5–8] min). The
711 recovery period was set to at least 2 h until the beginning of the behavioral session, with the aim of
712 minimizing the impact of anesthesia as much as possible. A solution of ^{18}F-FDG (ca. 74 MBq/0.4
713 mL) was intravenously injected just before the beginning of each behavioral session through the
714 indwelling catheter. After the 30-min session, the rats were returned to their home cage, and then a
715 30-min static PET scan was performed under anesthesia with 2.0–2.5% isoflurane 55 min after the
716 ^{18}F-FDG injection. During the PET scan, the body temperature of the anesthetized rats was
717 maintained at 37°C using a small animal warmer (BWT-100A, Bio Research Center, Nagoya,
718 Japan). The acquired emission data were sorted into a single sinogram and reconstructed by a
719 standard 2D filtered back projection (FBP) with a ramp filter and cutoff frequency at 0.5 cycles per
720 pixel or by a statistical maximum a *posteriori* probability algorithm (MAP), 12 iterations with point
721 spread function effect.

722 Voxel-based analysis of PET images was conducted according to the method described

723 previously (***Cui et al., 2015***). Briefly, individual MAP-reconstructed FDG images were aligned to a
724 FDG template image of Long Evans rats using PMOD software package (version 3.2; PMOD
725 Technologies, Fällanden, Switzerland; https://www.pmod.com/web/) and then the aligned images
726 were transformed into the space of a T2 weighted MRI templates for the Long-Evans rat brain
727 (Neuroimaging Tools and Resources Collaboratory; https://www.nitrc.org/projects/tpm_rat/). The
728 transformation parameters obtained from individual MAP-reconstructed FDG images were used to
729 match the individual FBP-reconstructed FDG images with the MRI templates. The voxel size of the
730 template was magnified by 10 to a size similar to that of a human brain. All FBP-reconstructed
731 FDG images were resampled with a voxel size of 1.2 × 1.2 × 1.2 mm and spatially smoothed
732 through an isotropic Gaussian kernel (6-mm FWHM). Voxel-based statistical analysis was
733 performed by using the Statistical Parametric Mapping (SPM) software (version 8; Wellcome
734 Department of Imaging Neuroscience, London, UK; https://www.fil.ion.ucl.ac.uk/spm/). For
735 visualization of the results, SPM t-statistic values were overlayed on MRI templates to define the
736 voxels showing significantly increased or decreased brain activity, using a high threshold (p =
737 0.001, uncorrected) and an extent threshold (with the output values from the voxel-based analysis).
738 The voxel of interest was determined ass voxels with more than 85% of the maximum T-value
739 within activated areas obtained by voxel-based statistical comparison of the FBP-FDG images. The
740 average regional ^{18}F-FDG uptake was calculated on the basis of values of the voxel of interest in the
741 images.
742
743 **Electrophysiological recording**
744 Extracellular multi-unit recording was conducted at a sampling rate of 20 kHz from the striatum of
745 freely moving rats by using a 512-ch acquisition board (Open Ephys, Atlanta, GA) via 64-ch
746 recording headstages (C3325, Intan Technologies, Los Angeles, CA). The tips of the probe were
747 lowered by turning the screw (> 140 μm/day) until it reached the target regions (the aDLS and
748 pVLS) during the single lever press task. The tips were sometimes lowered by the same procedure

749 (140 to 280 μm/day) after the daily recording session to improve cell yield. Spike sorting was
750 performed automatically by the Kilosort2 software (***Stringer et al., 2015;*** Marius Pachitariu,
751 Ashburn, VA; https://www.github.com/MouseLand/Kilosort2). Clear noise clusters were removed
752 in the first manual sorting using the phy software (cortex-lab, London, UK;
753 https://github.com/cortex-lab/phy). The remaining clusters were then re-clustered by using the
754 KlustaKwik2 software (***Kadir et al., 2014;*** https://github.com/kwikteam/klustakwik2), and the
755 clusters were adjusted in the second manual sorting by using the phy again. The sorted clusters
756 satisfying all the following criteria were used for further analysis: L-ratio < 0.05, isolation distance
757 > 15, and inter-spike interval (ISI) index < 0.2 (***Fee et al., 1996; Schmitzer-Torbert et al., 2005***).
758 Well-isolated single neurons (n = 1,485; aDLS, n = 1,062; pVLS, n = 423) were classified as
759 putative MSNs, fast spiking interneurons (FSIs), tonically active neurons (TANs), and unclassified
760 interneurons (UIs). Putative MSNs and TANs were separated from FSIs and UIs by trough-to-peak
761 duration of mean spike waveform (> 0.6 ms) according to previous studies with slight modifications
762 (***Bakhurin et al., 2016; Kim et al., 2019***). Putative FSIs were then separated from UIs by utilizing
763 the proportion of time associated with long ISIs. This was achieved by summing the ISIs longer
764 than 2 s and subsequently dividing the resulting sum by the total recording time ($Prop_{ISIs} > 2$ s)
765 (***Peters et al., 2021***). Neurons with values of $Prop_{ISIs} > 2$ s less than 0.4 were classified as putative
766 FSIs, while neurons with $Prop_{ISIs} > 2$ s greater than 0.4 were classified as putative UIs. The putative
767 MSNs and TANs were separated by measuring the post-spike suppression (***Peters et al., 2021***). We
768 measured the length of suppressed time during which the firing rate of a neuron was suppressed
769 following a spike by counting the number of 1-ms bins in its autocorrelation function until the rate
770 of the neuron was equal to or greater than its averaged rate over the 600-ms to 900-ms
771 autocorrelation bins. Putative TANs were separated by post-spike suppression of less than 40 ms,
772 and the remaining neurons were classified as putative MSNs.
773 To divide the three stages during the acquisition phase, the sigmoidal function was fitted
774 using the following four-parameter logistic equation:

$$f_{(x)} = \frac{1 - \gamma - (1 - \lambda)}{1 + \exp\left(-\beta(x - \alpha)\right)} + \gamma$$

Where α is the inflection point, β is a variable for slope, and λ and γ are parameters related to the lower asymptote and upper asymptote of the learning curve, respectively. The function was used to evaluate the day when the success rate reached 20% ($t_{20\%}$) or 90% ($t_{90\%}$) of the maximum rate change defined by the difference between the γ and λ. Three stages were defined according to the following criteria: early stage (up to 3 days before the middle stage); middle stage (3 days including before and after the day of $t_{20\%}$); and late stage (3 days including the day of $t_{90\%}$ and before). One rat learned the discrimination faster, and the success rate reached $t_{90\%}$ 2 days after the day of $t_{20\%}$. One day before the day of $t_{90\%}$ was assigned to the late stage. For the following analysis, spike data in each striatal subregion were separated into the early, middle, and late stages (n = 295, 364 and 360, respectively, for the aDLS; and n = 87, 110 and 190, respectively, for the pVLS).

To determine the neurons showing significant changes in firing rate related to the task events, electrophysiological data were grouped into four trial types based on the instruction cue (high or low tone) and the choice (right or left lever); HR, high tone and right lever press; LL, low tone and left lever press; HL, high tone and left lever press; and LR, low tone and right lever press. Neurons with three or more trial data were analyzed. We identified the HR or LL type neurons, detecting significant increases or decreases of the firing rate by applying the Wilcoxon rank-sum test ($p < 0.01$) to trial-by-trial spike number between the baseline period (BL, -1,500 to -500 ms or -1,100 to -500 ms before presentation of the instruction cue) and any of four peri-event periods (cue onset, 0 to +1,000 ms after the onset of the instruction cue; choice response, -700 to +300 ms around the time of lever press; reward sound, -300 to 300 ms around the time of sound onset instructing the reward delivery; and first licking, 0 to +1,000 ms after the time of first licking after the choice response). Any spikes around the events were averaged in 50-ms bins. The event-related activity was shown as averaged firing rate aligned based on the timing of an event for each trial. The auROC values were calculated by using the spike counts between one trial and either of the

other three trials. Bins showing significant differences in the auROC data were determined by applying the Wilcoxon rank-sum test ($p < 0.05$) to the distribution of 200 ms bin-by-bin auROC values and 0.5.

To compare the number of neurons showing event-related activity among different stages, the number of HR or LL type neurons were calculated by matching the trial number at each stage. Twenty trials were randomly selected for a neuron, and neurons with less than 20 trials were removed from the analysis. The neurons with event-related activity were identified as described above. The proportion (percentage) of neurons relative to the total number of neurons was calculated at each individual stage. The same analysis was repeated 30 times and the distribution of the proportion of neurons with event-related activity at the stage was obtained. The cumulative probability against the proportion was calculated using cumulative distribution function (cdfplot; MATLAB, MathWorks, Natick, MA).

Licking responses were detected with an infrared photobeam sensor placed in the 3D printed reward port, and generated timestamps for the onset of each spout contact according to the analog voltage signal. The licking responses corresponding to four kinds of trial in the first licking-related neurons were shown as averaged rates (50-ms bins) aligned based on the timing of the choice response. To calculate the correlation coefficient between neuronal activity and licking responses, the spikes and licking for 5 s after the first licking were counted every trial for each first licking-related neuron. Trials in which neurons never responded were removed from both the spike and licking data. The correlation coefficients between the two kinds of data were calculated for each neuron (corr; MATLAB, MathWorks), and neurons showing significant differences were determined by applying the Pearson correlation coefficient ($p < 0.01$).

Histology

After the behavioral experiments, rats were anesthetized with pentobarbital (50 mg/kg body weight) and isoflurane (3%), then transcardially perfused 4% paraformaldehyde in phosphate-buffer (PB).

826 The brains were post-fixed overnight at 4 °C and cryoprotect with 10, 20, and 30% sucrose in PB.
827 Brain tissues were cut into 30-μm sections by using a cryostat (CM3050 S, Leica Biosystems,
828 Wetzlar, Germany). To define the lesioned areas in the striatum, sections were immunostained with
829 a mouse anti-NeuN antibody (1:1,000 dilution; MAB377, Millipore, Burlington, MA), and then
830 with a goat anti-mouse IgG antibody conjugated with Alexa Fluor 488 (1:1,000 dilution; A-11029,
831 Thermo Fisher Scientific, Waltham, MA). The sections were counterstained with 0.3 μM 4',6-
832 diamidino-2-phenylindole (DAPI; 0.1 μg/mL, D1306, Thermo Fisher Scientific). For the transient
833 inactivation experiment, the positions of guide cannulae were confirmed by staining with 0.1%
834 cresyl violet solution (41021, Muto Pure Chemicals, Tokyo, Japan). For the electrophysiological
835 experiments, small lesions were made by applying an electrolytic current (3 μA, 10 s) through top
836 and bottom channels of each shank by using the stimulus isolator (A365, World Precision
837 Instruments, Sarasota, FL). Sections through the striatum were stained with a mouse anti-TH
838 antibody (1:1,000 dilution; MAB318-AF488, Millipore), and then with a goat anti-mouse IgG
839 antibody conjugated with Alexa Fluor 488 (1:1,000 dilution; Jackson Immunoresearch Laboratories,
840 West Grove, PA). The recording sites were verified by staining with DAPI and red fluorescent Nissl
841 stain solution (1:10,000/1:200 dilution; N21482, Thermo Fisher Scientific). For the tracing, sections
842 through the ventral midbrain were stained with a mouse anti-TH antibody (1:1,000 dilution), and
843 then with a donkey anti-mouse IgG antibody conjugated with Alexa Fluor 647 (1:1,000 dilution; A-
844 31571, Thermo Fisher Scientific). Fluorescence and immunostained signals were visualized under
845 fluorescence microscopes (BZ-X800, Keyence, Osaka, Japan) and confocal microscope (A1R,
846 Nikon, Osaka, Japan).
847
848 **Statistical analysis**
849 Statistical analysis was performed using MATLAB (MathWorks) and SPSS Statistics (version 27;
850 IBM, Armonk, NY). Comparisons of data between two groups were performed using the Student's
851 *t*-test (paired), the Wilcoxon signed rank test (paired), and the Wilcoxon rank-sum test (unpaired).

Comparisons of data among three groups were constructed using a one-way repeated measures ANOVA, two-way repeated measures ANOVA, or the Kruskal-Wallis test (without assuming normal distribution and homogeneity of variances). All statistical tests were two-sided. The Bonferroni post-hoc test and Mann–Whitney U-test with Bonferroni adjustment were carried out as needed to compare means. For boxplots, the data points below the lower (25th percentile) -1.5 interquartile range and above the upper (75th percentile) quartiles +1.5 interquartile range were regarded as outliers, and they are not included in the boxplots.

Acknowledgements

We thank Drs. Keiji Ota, Hikaru Yokoyama, and Sho Aoki for instructing the behavioral analysis and Dr. Hideyuki Matsumoto for technical advice and discussion. We thank the Research Support Platform, Osaka Metropolitan University Graduate School of Medicine for microscopic imaging. This work was supported by grants-in-aid for JSPS Fellows (19J01997, S.S.), Scientific Research (C) (21K11556, S.S.), and Scientific Research (B) (25K02365, K.K.) from the Japan Society for the Promotion of Science; a grant-in-aid for Scientific Research on Transformative Research Areas (A) Adaptive Circuit Census (21H05244, K.K.) from the Ministry of Education, Science, Sports, and Culture of Japan; the Grant for Casio Science Promotion Foundation, Takeda Science Foundation; and the Nakatomi Foundation (S.S.).

Author contributions

S.S., Y.C., and K.K. designed the study. S.S. performed the small-animal neuroimaging, multi-unit recordings, tracing studies, and pharmacological experiments with technical support from all authors; T.O., D.H., Y.W., H.O., K.H., and Y.C. assisted with the neuroimaging studies. K.N. performed the tracing study, and N.S. assisted with the immunostaining. H.M., T.K., and K.M. assisted with the multi-unit extracellular recordings. S.S. and K.K. wrote the manuscript with assistance from all coauthors.

878 **Declaration of interest**

879 The authors declare no competing interest.

880

881 **Data availability**

882 Source data files have been provided for all experiments reported in this manuscript. All other data
883 are available upon request. The datasets generated and analyzed in this study are deposited on
884 Mendeley data (DOI: 10.17632/ghzr838bdk.1).

885

886 ## References

887 Amita H, Kim HF, Smith MK, Gopal A, Hikosaka O. 2019. Neuronal connections of direct and
888 indirect pathways for stable value memory in caudal basal ganglia. *European Journal of*
889 *Neuroscience* **49**:712-725. DOI: 10.1111/ejn.13936, PMID: 29737578

890 Alexander GE, Crutcher MD. 1990. Functional architecture of basal ganglia circuits: neural
891 substrates of parallel processing. *Trends in Neuroscience* **13**:266-271. DOI: 10.1016/0166-
892 2236(90)90107-l, PMID: 1695401

893 Barnes TD, Kubota Y, Hu D, Jin DZ, Graybiel AM. 2005. Activity of striatal neurons reflects
894 dynamic encoding and recoding of procedural memories. *Nature* **437**:1158-1161.
895 DOI: 10.1038/nature04053, PMID: 16237445

896 Barnes TD, Mao JB, Hu D, Kubota Y, Dreyer AA, Stamoulis C, Brown EN, Graybiel AM. 2011.
897 Advance cueing produces enhanced action-boundary patterns of spike activity in the
898 sensorimotor striatum. *Journal of Neurophysiology* **105**:1861-1878.
899 DOI: 10.1152/jn.00871.2010, PMID: 21307317

900 Bathellier B, Tee SP, Hrovat C, Rumpel S. 2013. A multiplicative reinforcement learning model
901 capturing learning dynamics and interindividual variability in mice. *Proceedings of the*
902 *National Academy of Sciences of the United States of America.* **110**:19950-19955.
903 DOI: 10.1073/pnas.1312125110, PMID: 24255115

904 Bakhurin KI, Mac V, Golshani P, Masmanidis SC. 2016. Temporal correlations among functionally
905 specialized striatal neural ensembles in reward-conditioned mice. *Journal of Neurophysiology*
906 **115**:1521-1532. DOI: 10.1152/jn.01037.2015, PMID: 26763779
907 Bergstrom HC, Lipkin AM, Lieberman AG, Pinard CR, Gunduz-Cinar O, Brockway ET, Taylor
908 WW, Nonaka M, Bukalo O, Wills TA, Rubio FJ, Li X, Pickens CL, Winder DG, Holmes A.
909 2018. Dorsolateral striatum engagement interferes with early discrimination learning. *Cell*
910 *Reports* **23**:2264-2272. DOI: 10.1016/j.celrep.2018.04.081, PMID: 29791838
911 Chen, Z., Chen Z, Zhang ZY, Zhang W , Xie T, Li Y, Xu XH, Yao H. 2021. Direct and indirect
912 pathway neurons in ventrolateral striatum differentially regulate licking movement and nigral
913 responses. *Cell Reports* **37**:109847. DOI: 10.1016/j.celrep.2021.109847, PMID: 34686331
914 Cui Y, Toyoda H, Sako T, Onoe K, Hayashinaka E, Wada Y, Yokoyama C, Onoe H, Kataoka
915 Y, Watanabe Y. 2015. A voxel-based analysis of brain activity in high-order trigeminal pathway
916 in the rat induced by cortical spreading depression. *Neuroimage* **108**:17-22.
917 DOI: 10.1016/j.neuroimage.2014.12.047, PMID: 25536498
918 Dickinson A. 1995. Actions and habits -The development of behavioral autonomy. *Phylosophical*
919 *Transactions of the Royal Society B: Biological Sciences* **308**:67-78. DOI:
920 10.1098/rstb.1985.0010
921 Doyon J, Bellec P, Amsel R, Penhune V, Monchi O, Carrier J, Lehéricy S, Benali H. 2009.
922 Contributions of the basal ganglia and functionally related brain structures to motor learning.
923 *Behavioural Brain Research* **199**:61-75. DOI: 10.1016/j.bbr.2008.11.012, PMID: 19061920
924 Endepols H, Sommer S, Backes H, Wiedermann D, Graf R, Hauber W. 2010. Effort-based decision
925 making in the rat: an [18F]fluorodeoxyglucose micro positron emission tomography study. *The*
926 *Journal of Neuroscience* **30**:9708-9714. DOI: 10.1523/JNEUROSCI.1202-10.2010,
927 PMID: 20660253
928 Featherstone RE, McDonald RJ. 2004. Dorsal striatum and stimulus-response learning: lesions of
929 the dorsolateral, but not dorsomedial, striatum impair acquisition of a simple discrimination

task. *Behavioural Brain Research* **150**:15-23. DOI: 10.1016/S0166-4328(03)00218-3, PMID: 15033275

Featherstone RE, McDonald RJ. 2005. Lesions of the dorsolateral striatum impair the acquisition of a simplified stimulus-response dependent conditional discrimination task. *Neuroscience* **136**:387-395. DOI: 10.1016/j.neuroscience.2005.08.021, PMID: 16226388

Fee MS, Mitra PP, Kleinfeld D. 1996. Automatic sorting of multiple unit neuronal signals in the presence of anisotropic and non-Gaussian variability. *Journal of Neuroscience Methods* **69**:175-188. DOI: 10.1016/S0165-0270(96)00050-7, PMID: 8946321

Foster NN, Barry J, Korobkova L, Garcia L, Gao L, Becerra M, Sherafat Y, Peng B, Li X, Choi JH, Gou L, Zingg B, Azam S, Lo D, Khanjani N, Zhang B, Stanis J, Bowman I, Cotter K, Cao C, Yamashita S, Tugangui A, Li A, Jiang T, Jia X, Feng Z, Aquino S, Mun HS, Zhu M, Santarelli A, Benavidez NL, Song M, Dan G, Fayzullina M, Ustrell S, Boesen T, Johnson DL, Xu H, Bienkowski MS, Yang XW, Gong H, Levine MS, Wickersham I, Luo Q, Hahn JD, Lim BK, Zhang LI, Cepeda C, Hintiryan H, Dong HW. 2021. The mouse cortico-basal ganglia-thalamic network. *Nature* **598**:188-194. DOI: 10.1038/s41586-021-03993-3, PMID: 34616074

Gimenez TL, Lorenc M, Jaramillo S. 2015. Adaptive categorization of sound frequency does not require the auditory cortex in rats. *Journal of Neurophysiology* **114**:1137-1145. DOI: 10.1152/jn.00124.2015, PMID: 26156379

Gremel CM, Chancey JH, Atwood BK, Luo G, Neve R, Ramakrishnan C, Deisseroth K, Lovinger DM, Costa RM. 2016. Endocannabinoid modulation of orbitostriatal circuits gates habit formation. *Neuron* **90**:1312-1324. DOI: 10.1016/j.neuron.2016.04.043, PMID: 27238866

Guo L, Weems JT, Walker WI, Levichev A, Jaramillo S. 2019. Choice-selective neurons in the auditory cortex and in its striatal target encode reward expectation. *The Journal of Neuroscience* **39**:3687-3697. DOI: 10.1523/JNEUROSCI.2585-18.2019, PMID: 30837264

Hintiryan, H., Foster NN, Bowman I, Bay M, Song MY, Gou L Yamashita S, Bienkowski MS, Zingg B, Zhu M, Yang XW, Shih JC, Toga AW, Dong HW. 2016. The mouse cortico-striatal

projectome. *Nature Neuroscience* **19**:1100-1114. DOI: 10.1038/nn.4332, PMID: 27322419

Hunnicutt BJ, Jongbloets BC, Birdsong WT, Gertz KJ, Zhong H, Mao T. 2016. A comprehensive excitatory input map of the striatum reveals novel functional organization. *eLife* **5**:e19103. DOI: 10.7554/eLife.19103, PMID: 27892854

Jin X, Costa RM. 2010. Start/stop signals emerge in nigrostriatal circuits during sequence learning. *Nature* **466**:457-462. DOI: 10.1038/nature09263, PMID: 20651684

Jog MS, Kubota Y, Connolly CI, Hillegaart V, Graybiel AM. 1999. Building neural representations of habits. *Science* **286**:1745-1749. DOI: 10.1126/science.286.5445.1745, PMID: 10576743

Kadir SN, Goodman DFM, Harris KD. 2014. High-dimensional cluster analysis with the masked EM algorithm. *Neural Computation* **26**:2379-2394. DOI: 10.1162/NECO_a_00661, PMID: 25149694

Kim HF, Hikosaka O. 2013. Distinct basal ganglia circuits controlling behaviors guided by flexible and stable values. *Neuron* **79**:1001-1010. DOI: 10.1016/j.neuron.2013.06.044, PMID: 23954031

Kim HF, Hikosaka O. 2015. Parallel basal ganglia circuits for voluntary and automatic behaviour to reach rewards. *Brain* **138**:1776-1800. DOI: 10.1093/brain/awv134, PMID: 25981958

Kim N, Li HE, Hughes RN, Watson GDR, Gallegos D, West AE, Kim IH, Yin HH. 2019. A striatal interneuron circuit for continuous target pursuit. *Nature Communications* **10**:2715. DOI: 10.1038/s41467-019-10716-w, PMID: 31222009

Kitanishi T, Umaba R, Mizuseki K. 2021. Robust information routing by dorsal subiculum neurons. *Science Advances* **7**:eabf1913. DOI: 10.1126/sciadv.abf1913, PMID: 33692111

Kornblum, H.I., Araujo DM, Annala AJ, Tatsukawa KJ, Phelps ME, Cherry SR. 2000. In vivo imaging of neuronal activation and plasticity in the rat brain by high resolution positron emission tomography (microPET). *Nature Biotechnology* **18**:655-660. DOI: 10.1038/76509, PMID: 10835605

Kupferschmidt DA, Juczewski K, Cui G, Johnson KA, Lovinger DM. 2017. Parallel, but

982 dissociable, processing in discrete corticostriatal inputs encodes skill learning. *Neuron* **96**:476-
983 489.e5. DOI: 10.1016/j.neuron.2017.09.040, PMID: 29024667
984 Lee CC. 2013. Thalamic and cortical pathways supporting auditory processing. *Brain and*
985 *Language* **126**:22-28. DOI: 10.1016/j.bandl.2012.05.004, PMID: 22728130
986 Lee J, Wang W, Sabatini BL. 2020. Anatomically segregated basal ganglia pathways allow parallel
987 behavioral modulation. *Nature Neuroscience* **23**:1388-1398. DOI: 10.1038/s41593-020-00712-
988 5, PMID: 32989293
989 Lehéricy S. Benali H, Van de Moortele PF, Pélégrini-Issac M, Waechter T, Ugurbil K, Doyon J.
990 2005. Distinct basal ganglia territories are engaged in early and advanced motor sequence
991 learning. *Proceedings of the National Academy of Sciences of the United States of America.*
992 **102**:12566-12571. DOI: 10.1073/pnas.0502762102, PMID: 16107540
993 Marx C, Lex B, Calaminus C, Hauber W, Backes H, Neumaier B, Mies G, Graf R, Endepols H.
994 2012. Conflict processing in the rat brain: behavioral analysis and functional μPET imaging
995 using [^{18}F]fluorodeoxyglucose. *Frontiers in Behavioral Neuroscience* **6**:4.
996 DOI: 10.3389/fnbeh.2012.00004, PMID: 22363272
997 Miyachi S, Hikosaka O, Lu X. 2002. Differential activation of monkey striatal neurons in the early
998 and late stages of procedural learning. *Experimental Brain Research* **146**:122-126.
999 DOI: 10.1007/s00221-002-1213-7, PMID: 12192586
1000 Miyachi S, Hikosaka O, Miyashita K, Kárádi Z, Rand MK. 1997. Differential roles of monkey
1001 striatum in learning of sequential hand movement. *Experimental Brain Research* **115**:1-5.
1002 DOI: 10.1007/pl00005669, PMID: 9224828
1003 Nishizawa K, Fukabori R, Okada K, Kai N, Uchigashima M, Watanabe M, Shiota A, Ueda
1004 M, Tsutsui Y, Kobayashi K. 2012. Striatal indirect pathway contributes to selection accuracy of
1005 learned motor actions. *The Journal of Neuroscience* **32**:13421-13432.
1006 DOI: 10.1523/JNEUROSCI.1969-12.2012, PMID: 23015433
1007 Nonomura S, Nishizawa K, Sakai Y, Kawaguchi Y, Kato S, Uchigashima M, Watanabe

M, Yamanaka K, Enomoto K, Chiken S, Sano H, Soma S, Yoshida J, Samejima K, Ogawa M, Kobayashi K, Nambu A, Isomura Y, Kimura M. 2018. Monitoring and updating of action selection for goal-directed behavior through the striatal direct and indirect pathways. *Neuron* **99**:1302-1314.e5. DOI: 10.1016/j.neuron.2018.08.002, PMID: 30146299

O'Hare JK, Ade KK, Sukharnikova T, Van Hooser SD, Palmeri ML, Yin HH, Calakos N. 2016. Pathway-specific striatal substrates for habitual behavior. *Neuron* **89**:472-479. DOI: 10.1016/j.neuron.2015.12.032, PMID: 26804995

Packard MG, Hirsh R, White NM. 1989. Differential effects of fornix and caudate nucleus lesions on two radial maze tasks: evidence for multiple memory systems. *The Journal of Neuroscience* **9**:1465-1472. DOI: 10.1523/JNEUROSCI.09-05-01465.1989, PMID: 2723738

Paxinos G, Watson C. 1998. *The Rat Brain in Stereotaxic Coordinates.* 4th ed. San Diego, CA: Academic Press.

Peters AJ, Fabre JMJ, Steinmetz NA, Harris KD, Carandini M. 2021. Striatal activity topographically reflects cortical activity. *Nature* **591**:420-425. DOI: 10.1038/s41586-020-03166-8, PMID 33473213

Redgrave P, Rodriguez M, Smith Y, Rodriguez-Oroz MC, Lehericy S, Bergman H, Agid Y, DeLong MR, Obeso JA. 2010. Goal-directed and habitual control in the basal ganglia: implications for Parkinson's disease. *Nature Reviews Neurosciece* **11**:760-772. DOI: 10.1038/nrn2915, PMID: 20944662

Schmitzer-Torbert N, Jackson J, Henze D, Harris K, Redish AD. 2005. Quantitative measures of cluster quality for use in extracellular recordings. *Neuroscience* **131**:1-11. DOI: 10.1016/j.neuroscience.2004.09.066, PMID: 15680687

Seger CA, Cincotta CM. 2005. The roles of the caudate nucleus in human classification learning. *The Journal of Neuroscience* **25**:2941-2951. DOI: 10.1523/JNEUROSCI.3401-04.2005, PMID: 15772354

Smith ACW, Jonkman S, Difeliceantonio AG, O'Connor RM, Ghoshal S, Romano MF, Everitt

BJ, Kenny PJ. 2021. Opposing roles for striatonigral and striatopallidal neurons in dorsolateral striatum in consolidating new instrumental actions. *Nature Communications* **12**:5121. DOI: 10.1038/s41467-021-25460-3, PMID: 34433818

Smith KS, Graybie, AM. 2016. Habit formation coincides with shifts in reinforcement representations in the sensorimotor striatum. *Journal of Neurophysiology* **115**:1487-1498. DOI: 10.1152/jn.00925.2015, PMID: 26740533

Stringer C, Pachitariu M, Steinmetz N, Reddy CB, Carandini M, Harris KD. 2019. Spontaneous behaviors drive multidimensional, brainwide activity. *Science* **364**:255. DOI: 10.1126/science.aav7893, PMID: 31000656

Thorn CA, Atallah H, Howe M, Graybiel AM. 2010. Differential dynamics of activity changes in dorsolateral and dorsomedial striatal loops during learning. *Neuron* **66**:781-795. DOI: 10.1016/j.neuron.2010.04.036, PMID: 20547134

Toni I, Passingham RE. 1999. Prefrontal-basal ganglia pathways are involved in the learning of arbitrary visuomotor associations: a PET study. *Experimental Brain Research* **127**:19-32. DOI: 10.1007/s002210050770, PMID: 10424411

Valtcheva S, Venance L. 2016. Astrocytes gate Hebbian synaptic plasticity in the striatum. *Nature Communications* **7**:13845. DOI: 10.1038/ncomms13845, PMID: 27996006

Williams ZM, Eskandar EN. 2006. Selective enhancement of associative learning by microstimulation of the anterior caudate. *Nature Neuroscience* **9**:562-568. DOI: 10.1038/nn1662, PMID: 16501567

Wolff SBE, Ko R, Ölveczky BP. 2022. Distinct roles for motor cortical and thalamic inputs to striatum during motor skill learning and execution. *Science Advances* **8**:eabk0231. DOI: 10.1126/sciadv.abk0231, PMID: 35213216

Xiong Q, Znamenskiy P, Zador AM. 2015. Selective corticostriatal plasticity during acquisition of an auditory discrimination task. *Nature* **521**:348-351. DOI: 10.1038/nature14225, PMID: 25731173

1060 Yin HH, Knowlton BJ. 2006. The role of the basal ganglia in habit formation. *Nature Reviews*
1061 *Neuroscience* **7**:464-476. DOI: 10.1038/nrn1919, PMID: 16715055
1062 Yin HH, Knowlton BJ, Balleine BW. 2004. Lesions of dorsolateral striatum preserve outcome
1063 expectancy but disrupt habit formation in instrumental learning. *European Journal of*
1064 *Neuroscience* **19**:181-189. DOI: 10.1111/j.1460-9568.2004.03095.x, PMID: 14750976
1065 Yin HH, Mulcare SP, Hilário MRF, Clouse E, Holloway T, Davis M, Hansson AC, Lovinger
1066 DM, Costa RM. 2009. Dynamic reorganization of striatal circuits during the acquisition and
1067 consolidation of a skill. *Nature Neuroscience* **12**:333-341. DOI: 10.1038/nn.2261,
1068 PMID: 19198605
1069 Yin HH, Ostlund SB, Knowlton BJ, Balleine BW. 2005. The role of the dorsomedial striatum in
1070 instrumental conditioning. *European Journal of Neuroscience* **22**:513-523. DOI: 10.1111/j.1460-
1071 9568.2005.04218.x, PMID: 16045504
1072 Zimmer ER, Parent MJ, Souza DG, Leuzy A, Lecrux C, Kim HI, Gauthier S, Pellerin L, Hamel
1073 E, Rosa-Neto P. 2017. [^{18}F] FDG PET signal is driven by astroglial glutamate transport. *Nature*
1074 *Neuroscience* **20**:393-395. DOI: 10.1038/nn.4492, PMID: 28135241
1075

1076 # Figures and legends

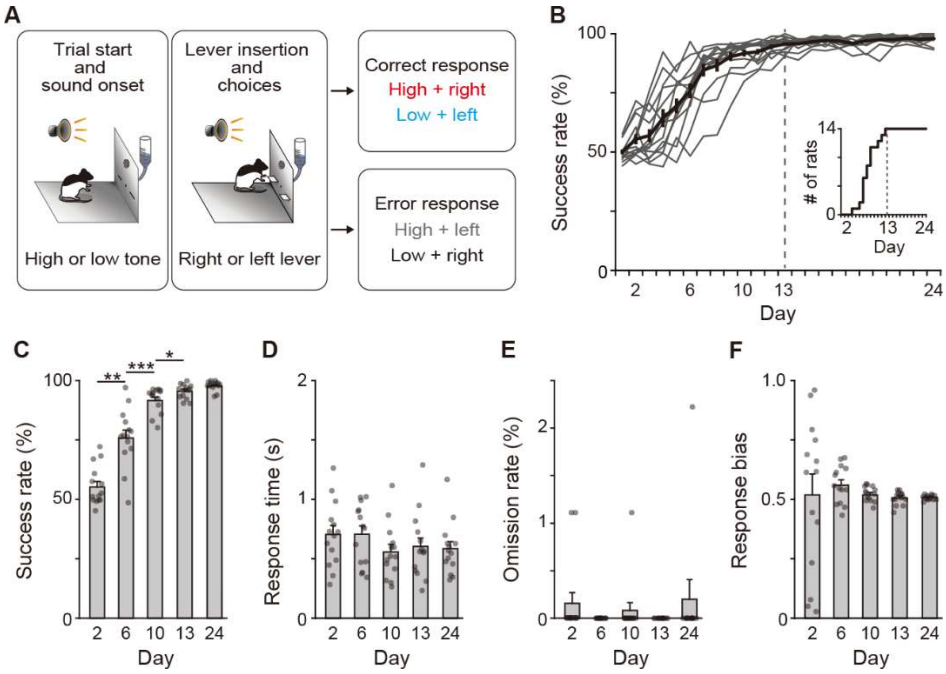

1077

1078 **Figure 1. Behavioral performance of two-alternative auditory discrimination learning.** (A)
1079 Schematic diagram of the auditory discrimination task. Each trial started by presentation of a tone
1080 instruction cue with the high (10 kHz) or low (2 kHz) frequency. Three seconds later, the room light
1081 was illuminated, and two retractable levers were inserted at the same time. The rats were required to
1082 press the right and left levers in response to the high and low tones, respectively. (B) Learning curve
1083 of the auditory discrimination in intact rats (n = 14). Inset indicates the cumulative curve of number
1084 achieved the success rate of more than 90%. (C) Success rate at Days 2, 6, 10, 13, and 24 (one-way
1085 repeated ANOVA, $F[1.897,24.659] = 106.706$, $p = 1.1 \times 10^{-12}$, *post hoc* Bonferroni test, Day 2 vs.
1086 Day 6, $p = 0.001$, Day 6 vs. Day 10, $p = 3.6 \times 10^{-4}$, Day 10 vs. Day 13, $p = 0.040$, and Day 13 vs.
1087 Day 24, $p = 0.080$). (D) Response time (one-way repeated ANOVA, $F[2.203,28.642] = 2.386$, $p =$
1088 0.105). (E) Omission rate ($F[4,52] = 0.699$, $p = 0.596$). (F) Response bias (one-way repeated
1089 ANOVA, $F[1.129,14.674] = 0.250$, $p = 0.653$). Data are indicated as the mean ± s.e.m., and
1090 individual data are overlaid. *$p < 0.05$, **$p < 0.01$, and ***$p < 0.001$.

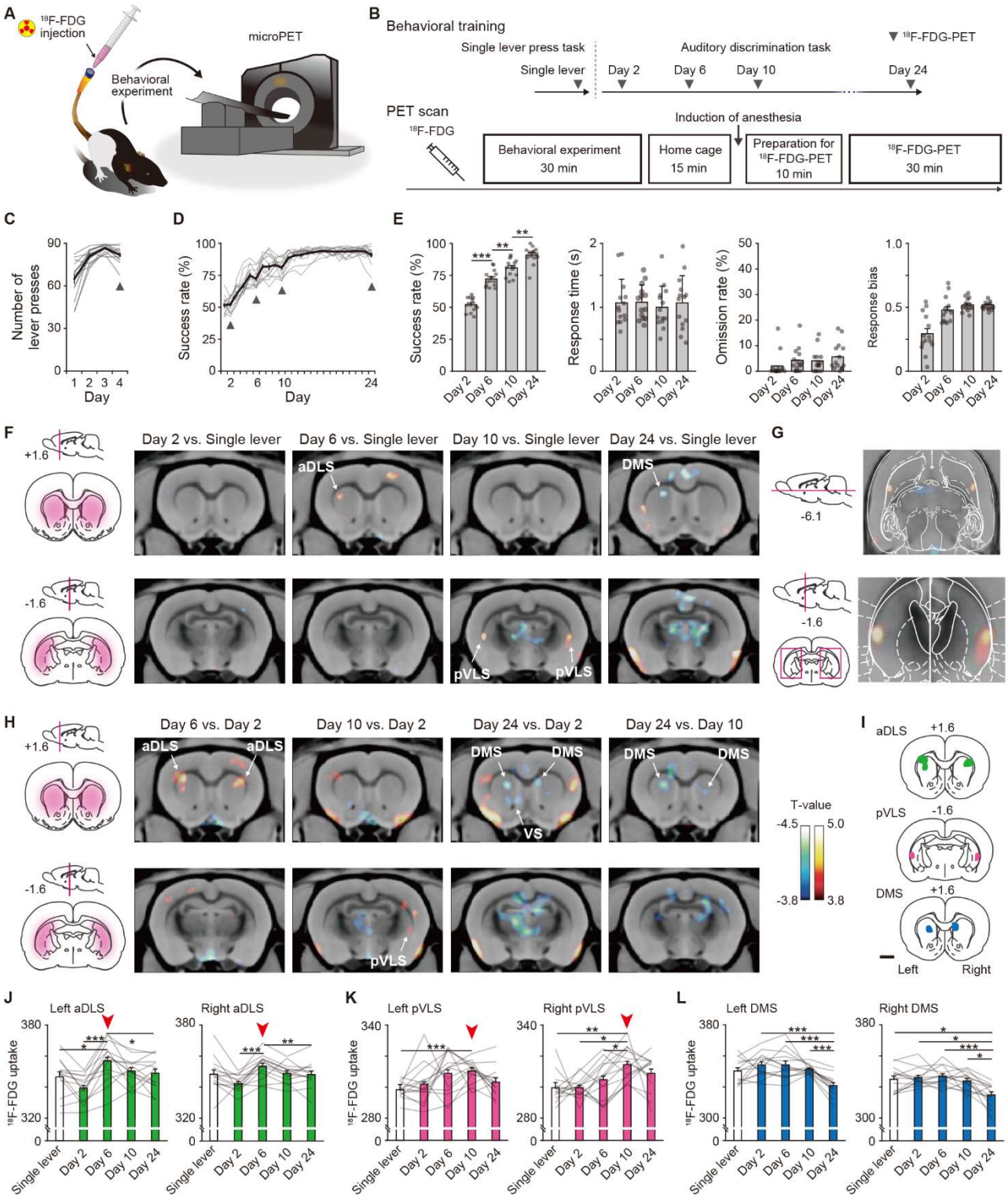

Figure 2. Dissociable brain activity patterns during auditory discrimination learning among three striatal subregions. (A) Schematic illustration of an awake rat received intravenously ^{18}F-FDG injection through an indwelling catheter attached to the tail. The rat was conducted for the behavioral experiment and then used for microPET imaging. (B) Schedule for the behavioral training and ^{18}F-FDG-PET scan. After ^{18}F-FDG injection, rats (n = 14 rats) were subjected to the

behavioral experiment (30 min) and returned to the home cage (15 min). Ten min before the PET scan started, the rats were anesthetized and then the scan was started (30 min). (C and D) Learning curves of the single lever press task (C) and auditory discrimination task (D). Arrowheads indicate the PET scan days. (E) Behavioral performance on the scan days during the auditory discrimination. Success rate (one-way repeated ANOVA, $F[3,39] = 125.012$, $p = 4.8 \times 10^{-20}$, *post hoc* Bonferroni test; Day 2 vs. Day 6, $p = 5.0 \times 10^{-7}$; Day 6 vs. Day 10, $p = 0.001$; Day 10 vs. Day 24, $p = 0.003$), response time (one-way repeated ANOVA, $F[3,39] = 0.156$, $p = 0.926$), omission rate (one-way repeated ANOVA, $F[3,39] = 1.559$, $p = 0.215$), and response bias (one-way repeated ANOVA, $F[1.779,23.130] = 17.734$, $p = 3.6 \times 10^{-5}$) are shown. (F) Representative images of coronal sections that compared the brain activity in the single lever press task with the activity on Day 2, 6, 10, or 24 in the discrimination task. Left panels show schematic illustrations of striatal subregions. (G) Horizontal (top) and coronal (bottom) images of striatal activation areas shown on Day 10 vs. single lever in (F). (H) Representative images of coronal section that compared the brain activity on Day 2 with that on Day 6, 10, or 24 in the discrimination task. Color bars indicate the T-values, and a value of 3.8 was used as the threshold corresponding to the uncorrected threshold ($p < 0.001$). (I) Schematic pictures showing voxel of interests for the aDLS, pVLS, and DMS. (J-L) Regional ^{18}F-FDG uptakes in the aDLS (J, one-way repeated ANOVA, left aDLS, $F[4,52] = 10.322$, $p = 3.0 \times 10^{-6}$, *post hoc* Bonferroni test; single lever vs. Day 6, $p = 0.016$; Day 2 vs. Day 6, $p = 6.5 \times 10^{-5}$; Day 2 vs. Day 10, $p = 0.019$; Day 2 vs. Day 24, $p = 0.017$; Day 6 vs. Day 24, $p = 0.041$; right aDLS, $F[4,52] = 7.462$, $p = 7.9 \times 10^{-5}$, *post hoc* Bonferroni test, Day 2 vs. Day 6, $p = 2.9 \times 10^{-4}$; Day 2 vs. Day 10, $p = 0.036$; Day 6 vs. Day 24, $p = 0.005$), pVLS (K, one-way repeated ANOVA, left pVLS, $F[2.368,30.784] = 4.152$, $p = 0.020$, *post hoc* Bonferroni test; single lever vs. Day 10, $p = 1.8 \times 10^{-5}$; right pVLS, $F[4,52] = 5.995$, $p = 4.8 \times 10^{-4}$, *post hoc* Bonferroni test, single lever vs. Day 10, $p = 0.001$; Day 2 vs. Day 10, $p = 0.011$; Day 6 vs. Day 10, $p = 0.032$), and DMS (L, one-way repeated ANOVA, left DMS, $F[4,52] = 12.836$, $p = 2.4 \times 10^{-7}$, *post hoc* Bonferroni test; Day 2 vs. Day 24, $p = 1.8 \times 10^{-5}$; Day 6 vs. Day 24, $p = 4.8 \times 10^{-4}$; Day 10 vs. Day 24, $p = 5.5 \times 10^{-5}$; right DMS,

$F[4,52] = 10.717$, $p = 2.0 \times 10^{-6}$, *post hoc* Bonferroni test; single lever vs. Day 24, $p = 0.036$; Day 2 vs. Day 24, $p = 0.011$; Day 6 vs. Day 24, $p = 2.6 \times 10^{-4}$; Day 10 vs. Day 24, $p = 0.011$). Arrowheads indicate the day with the most activations throughout the learning process. Data are indicated as the mean ± s.e.m., and individual data are overlaid. The anteroposterior coordinates from bregma (mm) are shown (F–I). Scale bar; 2 mm (I). *$p < 0.05$, **$p < 0.01$, and ***$p < 0.001$.

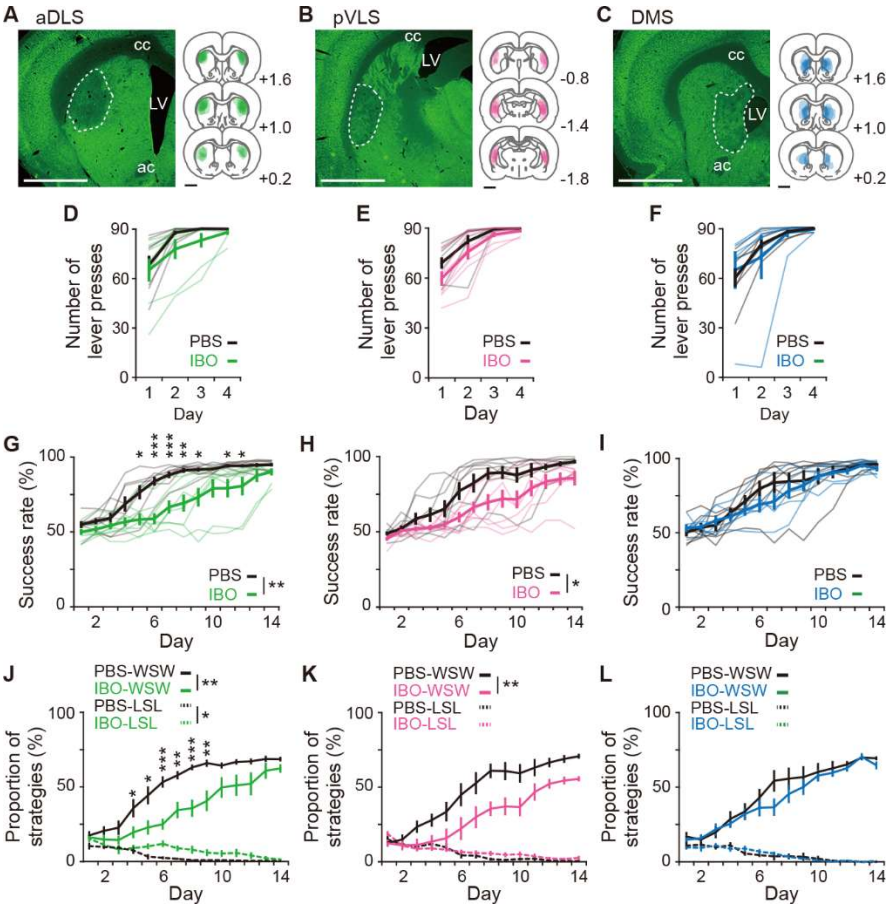

Figure 3. **Impacts of excitotoxic lesion of striatal subregions on the acquisition of auditory discrimination.** Rats were given intracranial injection of PBS or IBO solution into the aDLS (n = 8 for each injection), pVLS (n = 8 for each injection), or DMS (n = 7 for PBS injection, and n = 6 for IBO injection) before start of the single lever press task. (A-C) Representative images of NeuN immunostaining and individual schematic illustrations showing lesioned area in the aDLS (A), pVLS (B), or DMS (C). Dotted lines in the images indicate the range of the lesioned area. ac, anterior commissure; cc, corpus callosum; and LV, lateral ventricle. (D-F) Learning curves during the single lever press task in the groups injected into the aDLS (D, two-way repeated ANOVA, group, $F[1,14] = 1.275$, $p = 0.278$, day, $F[1.512,21.171] = 26.281$, $p = 7.0 \times 10^{-6}$, group × day, $F[1.512,21.171] = 0.834$, $p = 0.418$), pVLS (E, two-way repeated ANOVA, group, $F[1,14] = 2.542$, $p = 0.133$, day, $F[1.547,21.658] = 40.183$, $p = 2.2 \times 10^{-7}$, group × day, $F[1.547,21.658] = 0.953$, $p = 0.380$), or DMS (F, two-way repeated ANOVA, group, $F[1,11] = 0.025$, $p = 0.876$, day, $F[1.205,13.252] = 14.818$, $p = 0.001$, group × day, $F[1.205,13.252] = 0.610$, $p = 0.478$). (G-I)

Learning curves during the auditory discrimination task in the groups injected into the aDLS (G, two-way repeated ANOVA, group, $F[1,14] = 11.578$, $p = 0.004$, day, $F[2.805,39.274] = 60.733$, $p = 1.8 \times 10^{-14}$, group × day, $F[2.805,39.274] = 3.863$, $p = 0.018$, simple main effect, PBS vs. IBO, Day 1, $p = 0.140$, Day 2, $p = 0.085$, Day 3, $p = 0.284$, Day 4, $p = 0.068$, Day 5, $p = 0.011$, Day 6, $p = 9.5 \times 10^{-5}$, Day 7, $p = 0.001$, Day 8, $p = 0.002$, Day 9, $p = 0.012$, Day 10, $p = 0.059$, Day 11, $p = 0.034$, Day 12, $p = 0.046$, Day 13, $p = 0.136$, Day 14, $p = 0.096$), pVLS (H, two-way repeated ANOVA, group, $F[1,14] = 7.221$, $p = 0.018$, day, $F[3.646,51.041] = 51.794$, $p = 9.2 \times 10^{-17}$, group × day, $F[3.646,51.041] = 1.612$, $p = 0.190$), or DMS (I, two-way repeated ANOVA, group, $F[1,11] = 0.469$, $p = 0.507$, day, $F[2.677,29.452] = 48.860$, $p = 3.9 \times 10^{-11}$, group × day, $F[2.677,29.452] = 1.094$, $p = 0.362$). (J-L) Changes in the proportions of the win-shift-win or lose-shift-lose strategies through the discrimination learning in the groups treated into the aDLS (J, two-way repeated ANOVA, group, $F[1,14] = 13.451$, $p = 0.003$, day, $F[3.048,42.673] = 54.777$, $p = 9.1 \times 10^{-15}$, group × day, $F[3.048,42.673] = 3.288$, $p = 0.029$, simple main effect, PBS vs. IBO, Day 1, $p = 0.728$, Day 2, $p = 0.225$, Day 3, $p = 0.165$, Day 4, $p = 0.044$, Day 5, $p = 0.015$, Day 6, $p = 1.1 \times 10^{-4}$, Day 7, $p = 0.002$, Day 8, $p = 5.1 \times 10^{-4}$, Day 9, $p = 0.004$, Day 10, $p = 0.060$, Day 11, $p = 0.053$, Day 12, $p = 0.081$, Day 13, $p = 0.198$, Day 14, $p = 0.075$ for win-shift-win; group, $F[1,14] = 5.039$, $p = 0.041$, day, $F[3.866,54.119] = 14.578$, $p = 5.2 \times 10^{-8}$, group × day, $F[3.866,54.119] = 2.471$, $p = 0.057$ for lose-shift-lose), pVLS (K, two-way repeated ANOVA, group, $F[1,14] = 9.251$, $p = 0.009$, day, $F[3.206,44.881] = 47.168$, $p = 2.7 \times 10^{-14}$, group × day, $F[3.206,44.881] = 1.862$, $p = 0.146$ for win-shift-win; group, $F[1,14] = 0.762$, $p = 0.397$, day, $F[4.773,66.815] = 24.018$, $p = 1.9 \times 10^{-13}$, group × day, $F[4.773,66.815] = 1.338$, $p = 0.260$ for lose-shift-lose), or DMS (L, two-way repeated ANOVA, group, $F[1,11] = 0.703$, $p = 0.420$, day, $F[3.052,33.568] = 48.424$, $p = 2.3 \times 10^{-12}$, group × day, $F[3.052,33.568] = 0.846$, $p = 0.480$ for win-shift-win; group, $F[1,11] = 0.002$, $p = 0.965$, day, $F[3.442,37.866] = 13.787$, $p = 1.0 \times 10^{-6}$, group × day, $F[3.442, 37.866] = 0.581$, $p = 0.654$ for lose-shift-lose). Data are indicated as the mean ± s.e.m., and individual data are overlaid (except for panels J–L). The anteroposterior coordinates from bregma (mm) are shown (A–C). Scale bars; 2

1168 mm (A–C). *$p < 0.05$, **$p < 0.01$ and ***$p < 0.001$. Abbreviations: WSW, win-shift-win; and LSL,

1169 lose-shift-lose.

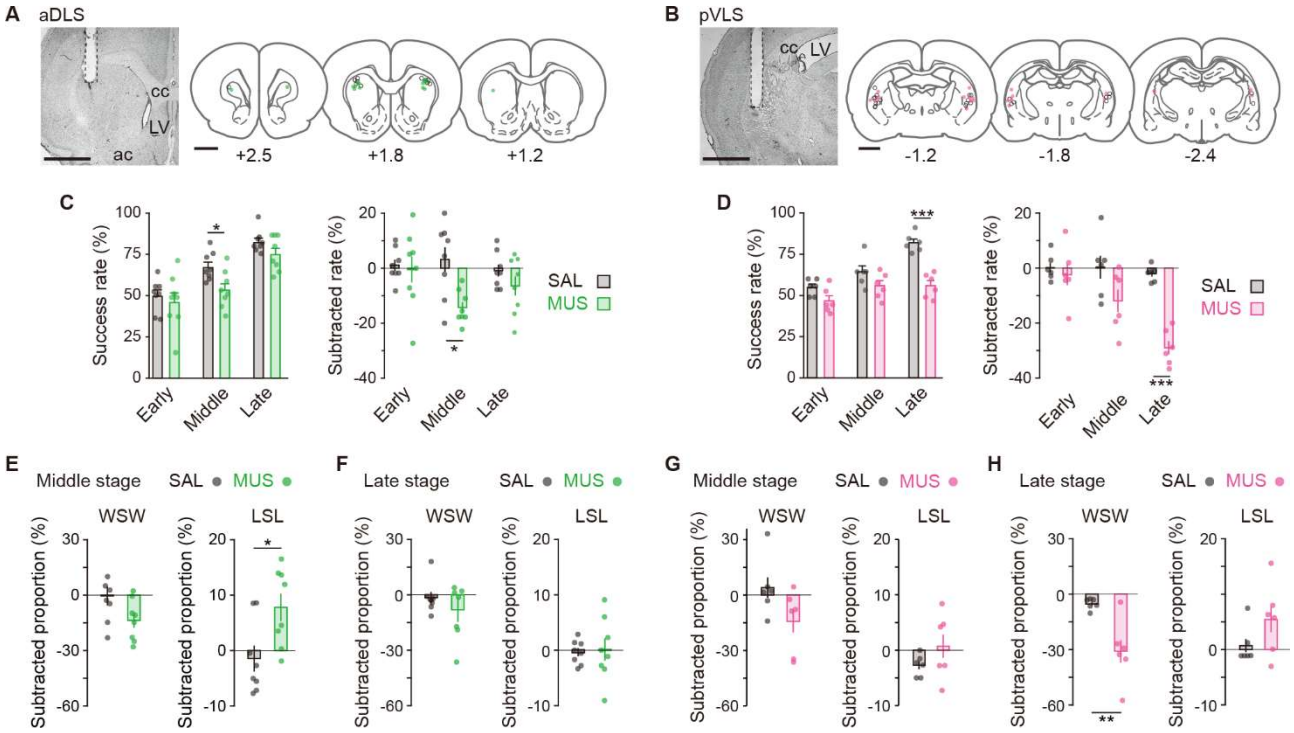

Figure 4. Influence of transient inhibition of striatal subregions at different timings on the performance of auditory discrimination. Rats received intracranial injection of SAL or MUS solution into the aDLS (n = 8 for each injection) or pVLS (n = 6 for each injection). (A and B) Representative images of cresyl violet staining and schematic illustrations showing placement sites of the tip of guide cannula in the aDLS (A) or pVLS (B). Dotted lines in the images indicate the position of the cannula placement. ac, anterior commissure; cc, corpus callosum; and LV, lateral ventricle. (C and D) Effects of transient striatal inhibition on the performance. For aDLS inhibition (C), success rate (left, two-way repeated ANOVA, stage, $F[2,28] = 28.708$, $p = 1.7 \times 10^{-7}$, group, $F[1,14] = 8.840$, $p = 0.010$, stage × group, $F[2,28] = 0.757$, $p = 0.478$; unpaired Student's t-test, early, $t[14] = 0.558$, $p = 0.586$; middle, $t[14] = 2.764$, $p = 0.015$; Welch's t-test, late, $t[12.010] = 1.617$, $p = 0.132$, $p = 0.016$ after a Bonferroni correction method) and subtracted success rate on day N-1 from that on day N (right, two-way repeated ANOVA, stage, $F[2,28] = 1.231$, $p = 0.307$, group, $F[1,14] = 10.797$, $p = 0.005$, stage × group, $F[2,28] = 2.360$, $p = 0.113$; unpaired Student's t-test, early, $t[14] = 0.285$, $p = 0.780$, late, $t[14] = 1.271$, $p = 0.225$, Welch's t-test, middle, $t[9.603] = 3.331$, $p = 0.008$, $p = 0.016$ after a Bonferroni correction method). For pVLS inhibition (D), success rate (left, two-way repeated ANOVA, stage, $F[2,20] = 17.642$, $p = 3.8 \times 10^{-5}$, group, $F[1,10] =$

43.942, $p = 5.9 \times 10^{-5}$, stage × group, $F[2,20] = 4.729$, $p = 0.012$; simple main effect, early, $p = 0.055$, middle, $p = 0.109$, late, $p = 4.2 \times 10^{-5}$) and subtracted success rate on day N-1 from that on day N (right, two-way repeated ANOVA, stage, $F[2,20] = 12.105$, $p = 3.6 \times 10^{-4}$, group, $F[1,10] = 16.310$, $p = 0.002$, stage × group, $F[2,20] = 8.500$, $p = 0.002$; simple main effect, early, $p = 0.595$, middle, $p = 0.085$, late, $p = 3.0 \times 10^{-6}$). (E and F) Subtracted proportion of the win-shift-win or lose-shift-lose strategies in the groups injected into the aDLS at the middle stage (E, unpaired Student's t-test, $t[14] = 2.038$, $p = 0.061$ for win-shift-win, and $t[14] = 2.714$, $p = 0.017$ for lose-shift-lose) and the late stage (F, unpaired Student's t-test, $t[14] = 0.898$, $p = 0.384$ for win-shift-win, and $t[14] = 0.226$, $p = 0.824$ for lose-shift-lose). (G and H) Subtracted proportion of the win-shift-win or lose-shift-lose strategies in the groups injected into the pVLS at the middle stage (G, unpaired Student's t-test, $t(10) = 1.924$, $p = 0.083$ for win-shift-win, and Welch's t-test, $t[6.095] = 1.364$, $p = 0.221$ for lose-shift-lose) and the late stage (H, unpaired Student's t-test, $t[10] = 3.629$, $p = 0.005$ for win-shift-win, and $t[10] = 1.577$, $p = 0.146$ for lose-shift-lose). Data are indicated as the mean ± s.e.m., and individual data are overlaid. The anteroposterior coordinates from bregma (mm) are shown (A and B). Scale bars; 2 mm (A and B). *$p < 0.05$, **$p < 0.01$, and ***$p < 0.001$. Abbreviations: WSW, win-shift-win; and LSL, lose-shift-lose.

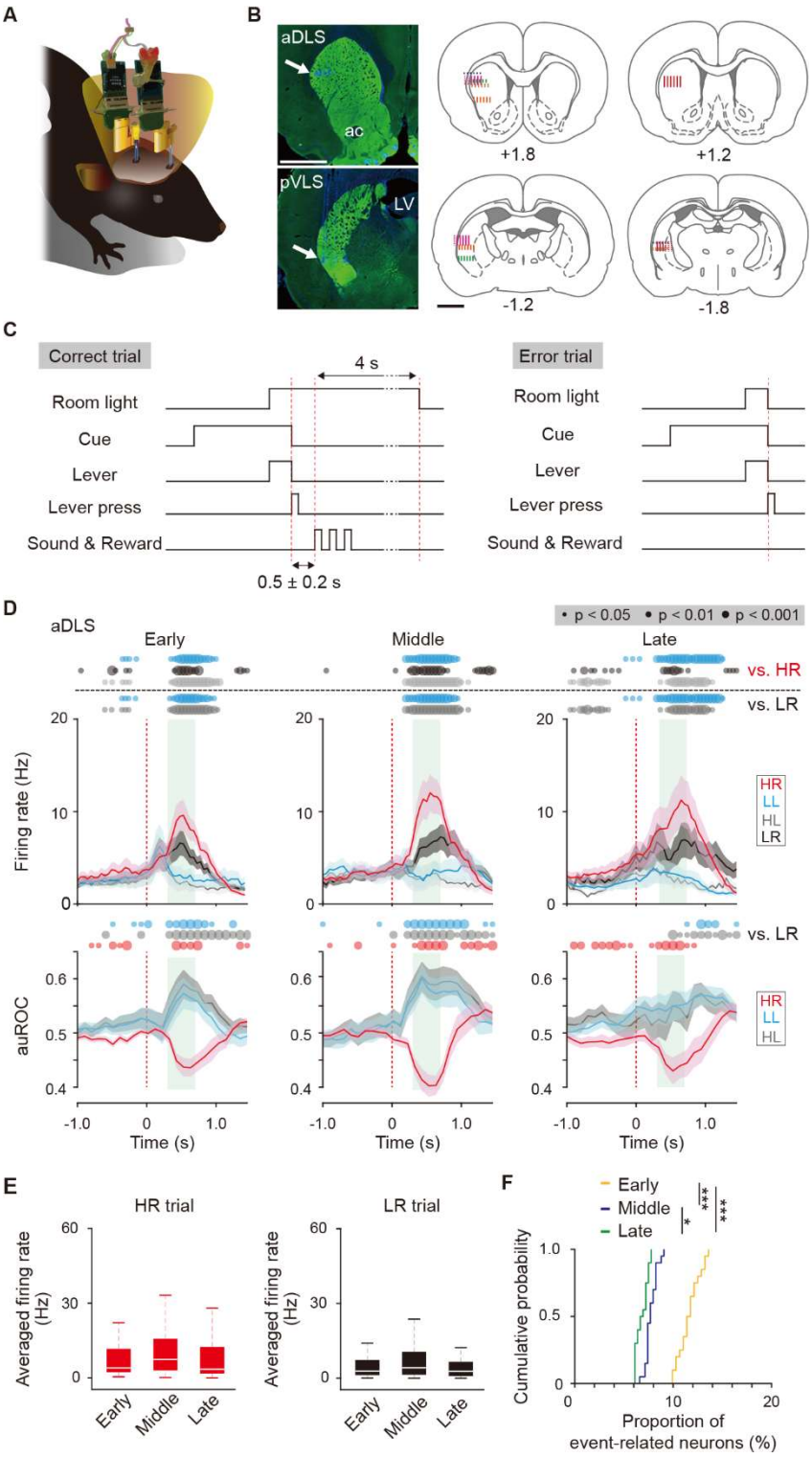

1203

1204 **Figure 5. Multi-unit recording of neurons in striatal subregions and firing activity related to**

1205 **the behavioral outcome of reward sound-related HR type neurons in the aDLS.** (A) Schematic

1206 illustration of a freely moving rat used for simultaneous multi-unit recordings in the aDLS and

1207 pVLS. Six rats were used for the following analysis. (B) Representative images of TH

1208 immunostaining, showing positions of electrode tips (arrows) in the aDLS and pVLS (left rows).

The recording sites estimated by electrode tracks and electrical marks in individual rats are shown (center and right rows). ac, anterior commissure; LV, lateral ventricle. (C) Sequence of some events in correct and error trials. The delay periods were pseudorandomly added between a correct lever press and the reward sound (0.5 ± 0.2 s). The room light turned off the extended time (4 s) after the correct response or immediately after the error response. (D) Mean firing rate (top rows) and auROC values (bottom rows) of reward sound-related HR type neurons in the aDLS at the early (n = 43 neurons), middle (n = 37 neurons), and late (n = 44 neurons) stages. These data are aligned to the choice response. Green shadows show the period when the reward sound is presented (500 ± 200 ms after the lever press). Time bins with significant differences between the mean firing rate in the HR or LR trial and any of the rates in other three trials (Wilcoxon signed rank test) or the distribution of auROC values and 0.5 (Wilcoxon rank-sum test) are represented by the circles at the top. (E) Averaged firing rate during the reward sound period in the HR and LR trials at the early, middle, and late stages (Kruskal-Wallis test: HR trial, $\chi^2 = 3.028$, $p = 0.220$; and LR trial, $\chi^2 = 1.249$, $p = 0.536$). (F) Cumulative probability of the proportion of reward sound-related HR type neuron number at the three stages (Kruskal-Wallis test, $\chi^2 = 45.378$, $p = 1.4 \times 10^{-10}$; *post hoc* Tukey-Kramer test, $p = 7.1 \times 10^{-5}$ for early vs. middle, $p = 1.0 \times 10^{-9}$ for early vs. late, and $p = 0.040$ for middle vs. late). Data are indicated as the mean ± s.e.m. (D) or the median and quartiles with the maximal and minimal values (E). The anteroposterior coordinates from bregma (mm) are shown (B). Scale bars; 2 mm (B). *$p < 0.05$ and ***$p < 0.001$.

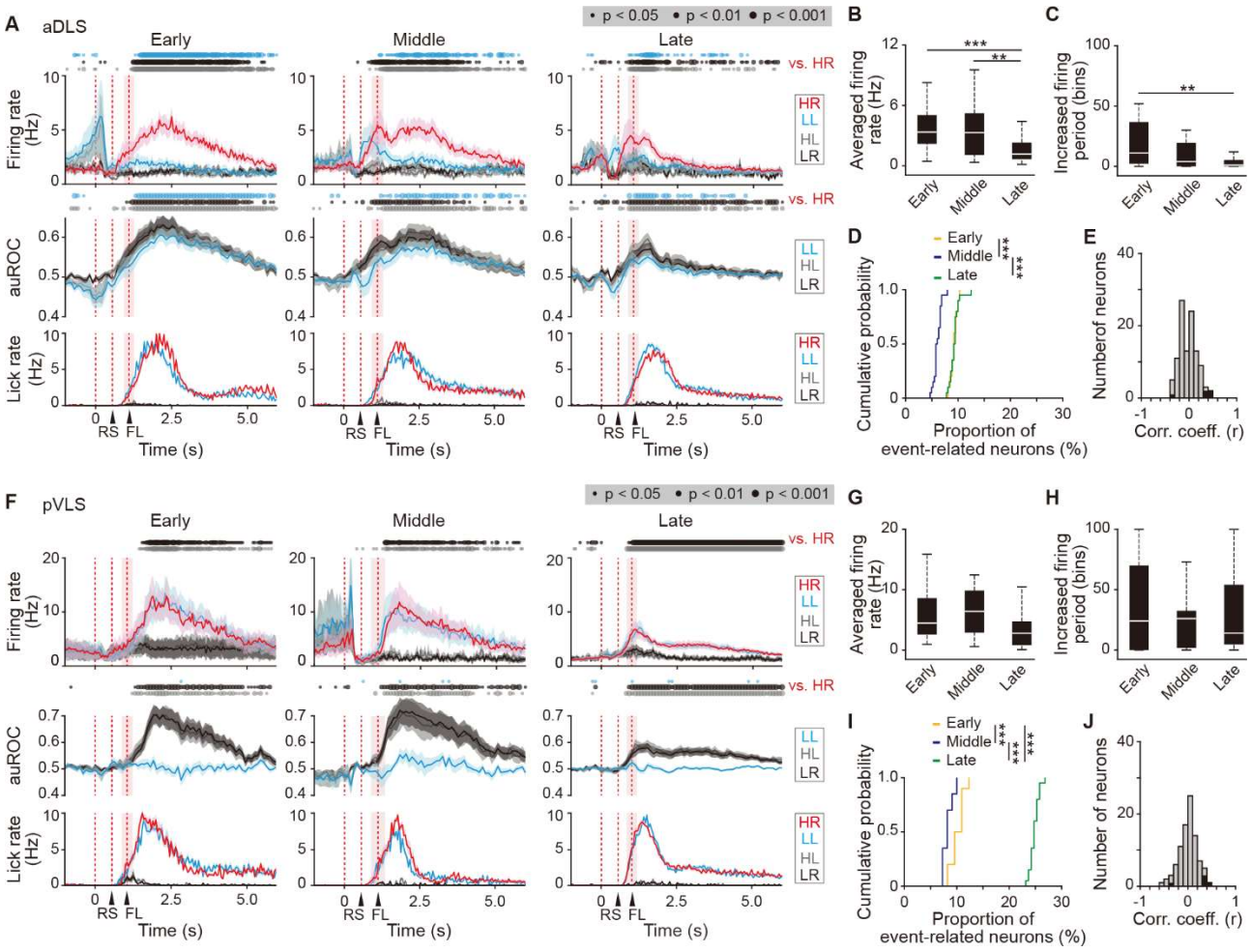

Figure 6. Sustained activity after the reward of first licking-related HR type neurons in the aDLS and pVLS. (A) Firing rate (top rows), auROC (middle rows), and licking rate (bottom rows) after the reward of first licking-related HR type neurons in the aDLS at the early (n = 27 neurons), middle (n = 31 neurons), and late (n = 49 neurons) stages. These data are aligned to the choice response. Timings of the reward sound and first licking are shown. Time bins with significant differences between the mean firing rate in the HR trial and any of the rate in other three trials (Wilcoxon signed rank test) or the distribution of auROC values and 0.5 (Wilcoxon rank-sum test) are represented by the circles at the top. (B) Averaged firing rate for 5 s after the first licking in the HR trial (Kruskal-Wallis test, $\chi^2 = 16.396$, $p = 2.8 \times 10^{-4}$, *post hoc* Tukey-Kramer test, early vs. middle, $p = 0.726$, early vs. late, $p = 7.2 \times 10^{-4}$, middle vs. late, $p = 0.009$). (C) Averaged total number of time bins above 3 s.d. of the baseline firing for 5 s after the first licking in the HR trial (Kruskal-Wallis test, $\chi^2 = 12.803$, $p = 0.002$, *post hoc* Tukey-Kramer test, early vs. middle, p =

0.173, early vs. late, $p = 0.001$, middle vs. late, $p = 0.219$). (D) Cumulative probability of the proportion of first licking-related HR type neuron number (Kruskal-Wallis test, $\chi^2 = 39.280$, $p = 3.0 \times 10^{-9}$, *post hoc* Tukey-Kramer test, early vs. middle, $p = 1.3 \times 10^{-7}$, early vs. late, $p = 0.995$, middle vs. late, $p = 2.3 \times 10^{-7}$). (E) Distribution of the correlation coefficient between the numbers of spikes and licking. Closed column indicates the number of neurons showing significant correlations between the two parameters (5 out of 107 neurons). (F) Firing rate (top rows), auROC (middle rows), and licking rate (bottom rows) after the reward of first licking-related HR neurons in the pVLS at the early ($n = 17$ neurons), middle ($n = 11$ neurons), and late ($n = 64$ neurons) stages. The data are aligned to the choice response, and the timings of the reward sound and first licking are shown. Time bins with significant differences between the rate in the HR trial and any of the rate in other trials or the distribution of auROC values and 0.5 are represented as above. (G) Averaged firing rate of pVLS neurons after the first licking in the HR trial (Kruskal-Wallis test, $\chi^2 = 7.652$, $p = 0.022$; *post hoc* Tukey-Kramer test, early vs. middle, $p = 0.975$, early vs. late, $p = 0.076$, and middle vs. late, $p = 0.096$). (H) Averaged total number of time bins above 3 s.d. of the baseline firing of pVLS neurons after the first licking in the HR trial (Kruskal-Wallis test, $\chi^2 = 0.023$, $p = 0.989$). (I) Cumulative probability of the proportion of first licking-related HR type neuron number (Kruskal-Wallis test, $\chi^2 = 47.922$, $p = 3.9 \times 10^{-11}$; *post hoc* Tukey-Kramer test, early vs. middle, $p = 0.011$, early vs. late, $p = 1.7 \times 10^{-4}$, and middle vs. late, $p = 9.7 \times 10^{-10}$). (J) Distribution of the correlation coefficient between the number of spikes and the licking. Closed column indicates the number of neurons showing significant correlations between the two parameters (5 out of 92 neurons). Data are indicated as the mean ± s.e.m. (A and F) or the median and quartiles with the maximal and minimal values (B, C, G, and H). $^{**}p < 0.01$ and $^{***}p < 0.001$. Abbreviations: RS, reward sound; and FL, first licking.

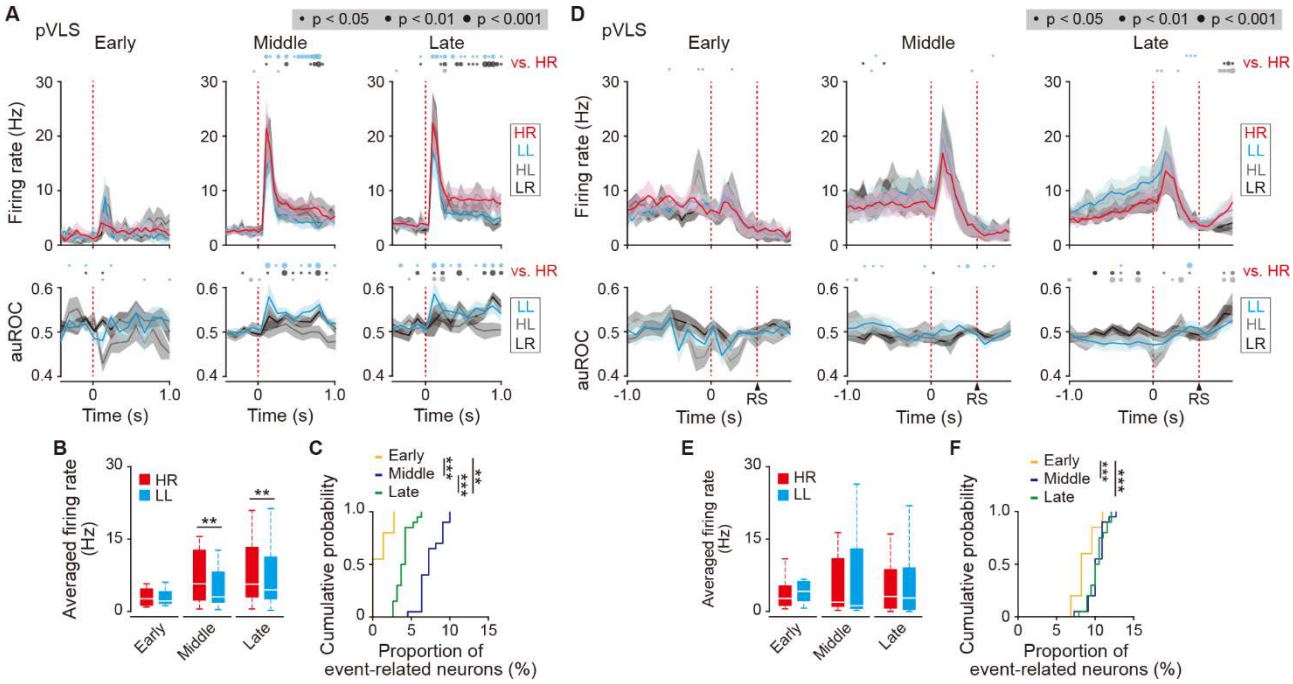

Figure 7. Transient activity related to the beginning and ending of a behavior of cue onset- and choice response-related HR type neurons in the pVLS. (A) Firing rate (top rows) and auROC values (bottom rows) of cue onset-related HR type neurons in the pVLS at the early (n = 4 neurons), middle (n = 21 neurons), and late (n = 24 neurons) stages. These data are aligned to the cue onset. Time bins with significant differences between the mean firing rate in the HR trial and either of the rate in other three trials (Wilcoxon signed rank test) or the distribution of auROC values and 0.5 (Wilcoxon rank-sum test) are represented by the circles at the top. (B) Averaged firing rate of the cue onset-related HR type neurons in HR and LL trials (0-600 ms after the cue onset) (Wilcoxon signed rank test; early, p = 0.875, middle, p = 0.006, and late, p = 0.004). (C) Cumulative probability of the proportion of the cue onset-related HR type neuron number (Kruskal-Wallis test, χ^2 = 51.114, $p = 8.0 \times 10^{-12}$; *post hoc* Tukey-Kramer test, early vs. middle, $p = 9.6 \times 10^{-10}$, early vs. late, p = 0.002, and middle vs. late, $p = 6.4 \times 10^{-4}$). (D) Firing rate (top rows) and auROC values (bottom rows) of the choice response-related HR type neurons in the pVLS at the early (n = 11 neurons), middle (n = 22 neurons), and late (n = 41 neurons) stages. These data are aligned to the choice response. The timing of the reward sound is presented. Time bins with significant differences between the mean rate in the HR trial and any of the rate in other trials or the

distribution of auROC values and 0.5 are represented as above. (E) Averaged firing rate of the choice response-related HR type neurons in HR and LL trials (0-600 ms after the choice response) (Wilcoxon signed rank test; early, $p = 0.278$, middle, $p = 0.758$, and late, $p = 0.279$). (F) Cumulative probability of the proportion of the choice response-related HR type neuron number (Kruskal-Wallis test, $\chi^2 = 13.786$, $p = 0.001$; *post hoc* Tukey-Kramer test, early vs. middle, $p = 0.003$, early vs. late, $p = 0.005$, and middle vs. late, $p = 0.976$). Data are indicated as the mean ± s.e.m. (A and D) or the median and quartiles with the maximal and minimal values (B and E). $^{**}p < 0.01$ and $^{***}p < 0.001$. Abbreviation: RS, reward sound.

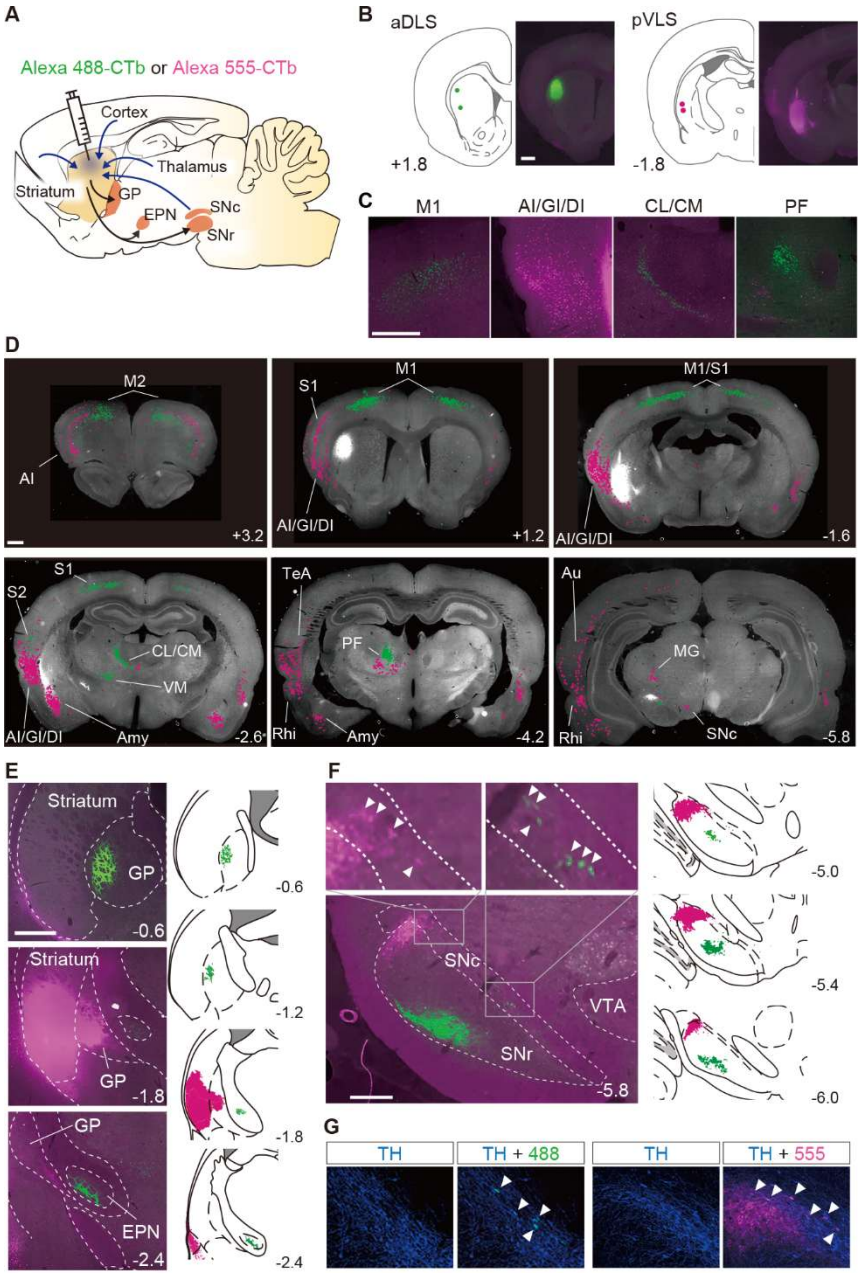

Figure 8. **Segregation of neural circuits linked to the aDLS and pVLS.** (A) Schematic illustration of the major inputs to and outputs from the striatum. A solution containing CTb labeled with Alexa 488 (green) or Alexa 555 (magenta) was injected into the aDLS and pVLS of the same animals (n = 2). (B) Coordinates for tracer injection into the aDLS and pVLS. Right, representative fluorescence images of sections through the injection sites. (C) Typical images of sections through the cerebral cortex and intralaminar thalamus. (D) Distribution of cell bodies innervating the aDLS and pVLS. Fluorescence signals in the cell bodies were marked by green or magenta dots using ImageJ (version 1.53) and overlaid on gray-scaled images of a brain section. (E) Axonal terminals

1299 arising from the aDLS and pVLS to the GP or EPN. Representative images of tracing are shown in
1300 the left panels. Camera lucida drawings of labeled signals are shown in the right panels. (F)
1301 Labeling of axonal terminals and cell bodies in the ventral midbrain. Representative images are
1302 shown in the left panels. Upper images are magnified views of the rectangles in the lower image.
1303 Camera lucida drawings are shown in the right panels. Arrowheads in the magnified images indicate
1304 labeled cell bodies. (G) Triple-fluorescence histochemistry with sections through the ventral
1305 midbrain. The sections were stained with an anti-TH antibody and then with a secondary IgG
1306 conjugated with Alexa 647. Representative images of the centromedial (left) and lateral (right) parts
1307 of the SNc are shown. Arrowheads indicate TH-positive cells with CTb-labeled signals in each
1308 image. The anteroposterior coordinates from bregma (mm) are shown. Scale bars; 1 mm (B-D), 500
1309 μm (E), 100 μm (F and G). Abbreviations: AI, agranular insular cortex; Amy, amygdala nucleus;
1310 Au, auditory cortex; CL, centrolateral nucleus; CM, centromedian nucleus; DI, dysgranular insular
1311 cortex; GI, granular insular cortex; M1, primary motor cortex; M2, secondary motor cortex; MG,
1312 medial geniculate nucleus; PF, parafascicular nucleus; Rhi, rhinal cortex; S1, primary
1313 somatosensory cortex; S2, secondary somatosensory cortex; TeA, temporal association cortex; VM,
1314 ventromedial nucleus; and VTA, ventral tegmental area.
1315

1316 **Author information**

1317 Susumu Setogawa

1318 Department of Physiology, Osaka Metropolitan University Graduate School of Medicine, Osaka 545-

1319 8585, Japan

1320 ORCID: 0000-0002-9161-2656

1321

1322 Takashi Okauchi

1323 Laboratory for Biofunction Dynamics Imaging, RIKEN Center for Biosystems Dynamics Research,

1324 Kobe 650-0047, Japan4Japan Society for the Promotion of Science, Tokyo 102-0083, Japa

1325

1326 Di Hu

1327 Department of Neurophysiology, Graduate School of Biomedical & Health Sciences, Hiroshima

1328 University, Hiroshima 734-8553, Japan

1329

1330 Yasuhiro Wada

1331 Laboratory for Pathophysiological and Health Science, RIKEN Center for Biosystems Dynamics

1332 Research, Kobe 650-0047, Japan

1333 ORCID: 0000-0003-2096-1602

1334

1335 Keigo Hikishima

1336 Medical Devices Research Group, Health and Medical Research Institute, National Institute of

1337 Advanced Industrial Science and Technology (AIST), Tsukuba 305-8564, Japan

1338 ORCID: 0000-0003-1133-1297

1339

1340 Hirotaka Onoe

1341 Human Brain Research Center, Kyoto University Graduate School of Medicine, Kyoto 606-8507,

1342 Japan

1343

1344 Kayo Nishizawa

1345 Department of Molecular Genetics, Institute of Biomedical Sciences, Fukushima Medical University

1346 School of Medicine, Fukushima 960-1295, Japan

1347 ORCID: 0009-0002-8398-588X

1348

1349 Nobuyuki Sakayori

1350 Department of Physiology and Oral Physiology, Graduate School of Biomedical and Health Sciences,

1351 Hiroshima University, Hiroshima 734-8553, Japan

1352 ORCID: 0000-0003-1611-4187

1353

1354 Hiroyuki Miyawaki

1355 Department of Physiology, Osaka Metropolitan University Graduate School of Medicine, Osaka 545-

1356 8585, Japan

1357 ORCID: 0000-0003-1556-1348

1358

1359 Takuma Kitanishi

1360 Department of Physiology, Osaka City University Graduate School of Medicine, Osaka 545-8585,

1361 Japan

1362 ORCID: 0000-0001-8062-3854

1363

1364 Kenji Mizuseki

1365 Department of Physiology, Osaka Metropolitan University Graduate School of Medicine, Osaka 545-

1366 8585, Japan

1367 ORCID: 0000-0002-1456-2149

1368 Yilong Cui

1369 Laboratory for Biofunction Dynamics Imaging, RIKEN Center for Biosystems Dynamics Research,

1370 Kobe 650-0047, Japan[4]Japan Society for the Promotion of Science, Tokyo 102-0083, Japan

1371 ORCID: 0000-0002-8302-1899

1372

1373 Kazuto Kobayashi

1374 Department of Molecular Genetics, Institute of Biomedical Sciences, Fukushima Medical University

1375 School of Medicine, Fukushima 960-1295, Japan

1376 ORCID: 0000-0002-7617-2939